University of Bristol - Explore Bristol Research
General rights

CrossMark

Impact of channelized flow on temperature distribution and fluid flow in restless calderas: Insight from Campi Flegrei caldera, Italy

Alia Jasim *, Fiona F. Whitaker, Alison C. Rust

School of Earth Sciences, University of Bristol, Bristol, UK

ABSTRACT

Magmatic hydrothermal systems develop by the imposition of a magmatically derived heat flux upon a shallow groundwater system. As such their dynamics can be intermittently perturbed by changing conditions within the associated magmatic system. Understanding the nature of the coupling between the magmatic and groundwater systems is thus key to discriminating geophysical signals of magmatic unrest from purely hydrothermal ones. Using a series of numerical groundwater models run with TOUGH2, we simulate the coupled groundwater–magmatic system at Campi Flegrei caldera, with particular emphasis on the impact of permeability developed within local fault systems and the dynamics of the system during magmatic unrest. Simulation results suggest that faults can play an important role in controlling the dynamics of recharge and heat transport within the shallow hydrothermal reservoir. Results specifically highlight that contrasts in permeability between faults and surrounding rock impact local temperature gradients, with faults either acting as preferential routes for recharge or discharge of groundwater, depending on fault/caldera fill permeability contrast and the vertical extent of the fault. Simulations of magmatic unrest with a step-wise increase in basal heat flux suggest that periodic geophysical and chemical signals may stem from the interaction between the development of gas at depth and the recharge–discharge dynamics of the reservoir. These results highlight the potential for the dynamics of magmatic–hydrothermal systems to be significantly impacted by the presence and nature of local fault systems. Where dynamic groundwater systems are involved, it is thus important to understand the impact of such geological elements when interpreting monitoring data such as ground deformation, seismicity and gas emissions.

© 2015 The Authors. Published by Elsevier B.V. This is an open access article under the CC BY-NC-ND license (http://creativecommons.org/licenses/by-nc-nd/4.0/).

1. Introduction

The pattern of long periods of quiescence punctuated by high magnitude events typical of caldera forming volcanoes (Di Vito et al., 1999; Lipman, 2007; Gottsmann and Marti, 2008) is a hazardous combination because there are limited opportunities for scientists to observe the escalation of magmatic activity in such systems. Furthermore, the low perceived risk of eruption often leads to the development of populated areas inside volcanic calderas. For example the Campi Flegrei caldera (CFc) has a population of more than 300,000 people, excluding the adjacent city of Naples (about 1 million people), and evacuation of the town of Pozzuoli during the 1982–1984 unrest crisis (1.5 m of uplift) involved 40,000 people.

Caldera forming volcanoes such as CFc often show extensive hydrothermal circulation (Dzurisin and Newhall, 1984; Gottsmann and Marti, 2008) and changes in hydrothermal activity could be important indicators of changes in a magmatic system. Therefore monitoring hydrothermal systems could be a useful tool for volcanic risk mitigation but it is essential to differentiate shallow hydrothermal signals from deeper, magmatic causes of unrest. The intensity of caldera hydrothermal systems likely arises from the combination of the high heat flux and the complexity of the structure and distribution of the caldera fill. Given the relative paucity of subsurface data, modelling studies aimed at understanding subsurface flow of heat and fluids are needed to augment surface observations such as ground deformation and fumarole activity. Although numerical simulations inevitably involve simplifications, they provide an important tool to explore our understanding of processes. However, it is important to include sufficient geological complexity in the distribution of permeability as it plays a key role in controlling fluid transport and the relative contributions of conduction and advection of heat.

Complexities in the permeability structure of calderas stem from structural features including faults as well as heterogeneities and facies changes in volcanic deposits. In high enthalpy areas, faults often discharge hot fluids to the surface (Kilty et al., 1979; Murphy, 1979; Bodvarsson et al., 1982; Goyal and Narasimhan, 1982). Hydrodynamic imbalance between cooler, denser water and more buoyant hot water sustains free convection. However it is unclear whether, in the absence

* Corresponding author at: School of Earth Sciences, University of Bristol, Wills Memorial Building, Queens Road, Bristol BS8 1RJ, UK. Tel.: +44 1179545246.
E-mail addresses: alia.jasim@bristol.ac.uk (A. Jasim), fiona.whitaker@bristol.ac.uk (F.F. Whitaker), alison.rust@bristol.ac.uk (A.C. Rust).

of a pressurised reservoir, faults preferentially discharge fluids or, contrastingly, allow cooling of the hydrothermal reservoir, enhancing the contribution of the cool shallow portion of the aquifer to the hydrothermal circulation. In any case faults seem key in distributing mass and heat in the subsurface with implications for local temperature gradients and surficial fluid discharge. The magnitude and anisotropy of the permeability of the caldera fill may also have large effects on hydrothermal circulation. The fill is either characteristically relatively permeable (Heap et al., 2014) or, if welded, the caldera fill permeability, especially the vertical component (Peluso and Arienzo, 2007; Wright and Cashman, 2014), is reduced and secondary permeability due to fractures is important (Chelini and Sbrana, 1987).

Building on previous numerical modelling studies simulating coupled magmatic–hydrothermal systems, we have explored the impact of adding faults and permeability anisotropy. The basis of our simulations is the system modelled by Todesco et al. (2010): a steady state convective flow system in which the injection of hot fluids feeds a narrow plume. This plume entrains water from the surrounding aquifer, depressing isotherms by up to 500 m in the zone of recharge. This baseline scenario (no faults) has been developed to match monitoring data (CO_2/H_2O ratio, ground deformation dynamics and gravity signals) at Campi Flegrei. The hydrothermal system is fed by fluids of magmatic origin, and unrest corresponds to periods of increased magmatic degassing (Chiodini et al., 2003; Todesco et al., 2010; Rinaldi et al., 2011). However the strong horizontal temperature anisotropy within

the caldera, as well as the localised hydro/magmatic phenomena, suggest that channelized flow plays a key role in distributing heat and mass in the shallow portion of the caldera. Thus we investigate the effect of faulting in the recharge dynamics of a hydrothermal system, with geometries, structures, permeabilities and fluids based on the Campi Flegrei caldera. A reference system is then perturbed to show the temporal evolution of magmatic unrest at Campi Flegrei. Vent opening and replenishment of a magmatic reservoir are simulated by injecting fluids at the faults and by increasing heat flux at the base of the model domain. These simulations help us to understand the conditions that may lead to the development of stable localised hot plume as well as to constrain the temporal response of the hydrothermal system to magmatic activity.

2. Regional setting

The complex nested caldera of Campi Flegrei (Naples, Italy) (Fig. 1) forms an approximately circular shape, 12 by 15 km across, with the longer axis oriented NW–SE. Orsi et al. (2004) identify three periods in the history of volcanism, with at least 70 eruptive events during the Quaternary. The first period started at least 60 ka ago and culminated with the emplacement of the Campanian Ignimbrite (39 ka, Barberi et al., 1978; Fisher et al., 1993; Rosi et al., 1996, 1999; Civetta et al., 1997; De Vivo et al., 2001). This was followed by a second period which ended with the smaller caldera collapse that emplaced the
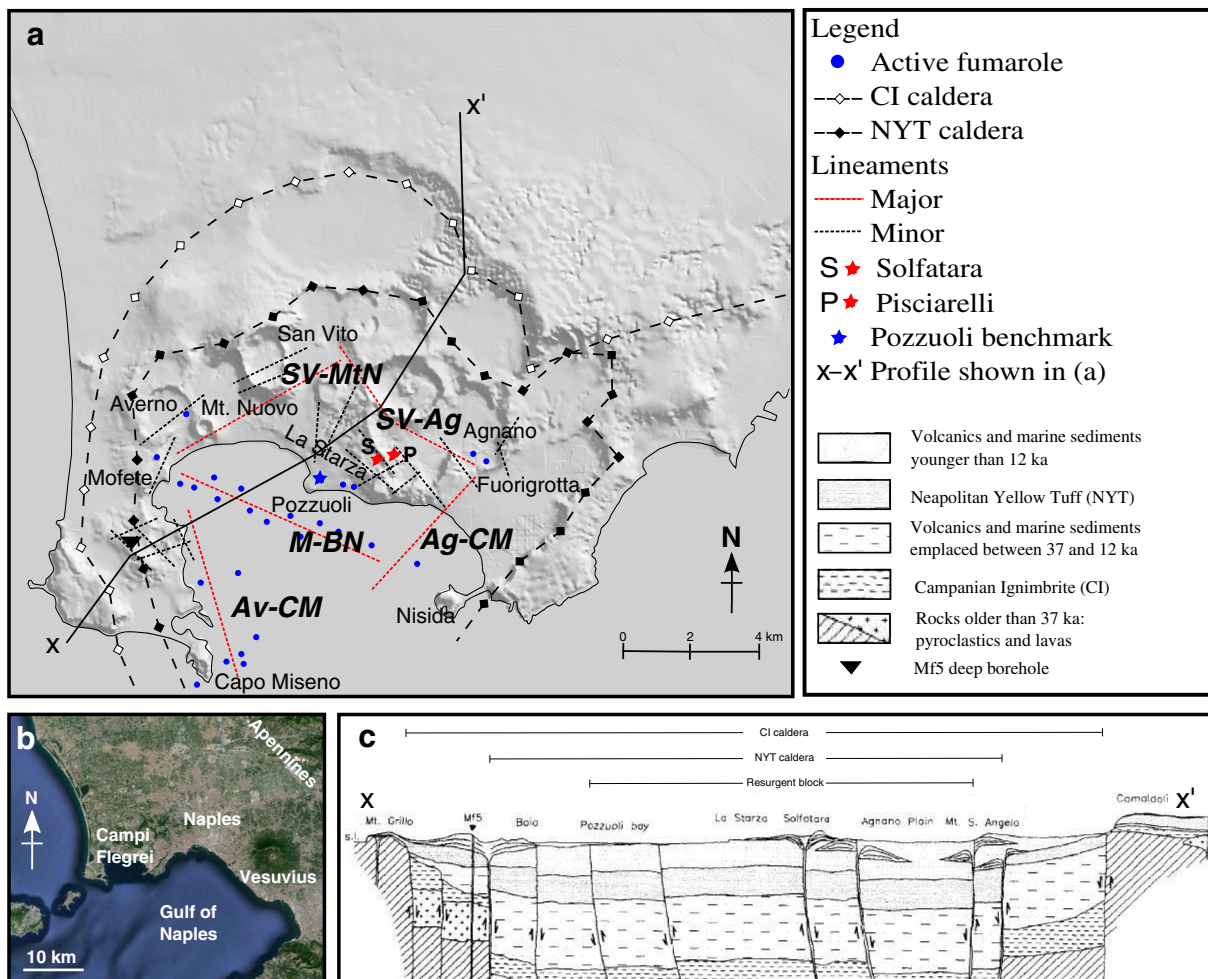
Fig. 1. a) Geological structures at Campi Flegrei caldera. The major lineaments highlighted in red are the San Vito–Agnano (SV–Ag), Mofete–Banco di Nisida (M–BN) and Averno–Capo Miseno (Av–CM), all showing Apenninic direction. Perpendicular to these are the San Vito–Mt. Nuovo (SV–MtN) and Agnano–Capo Miseno (Ag–CM) alignments (modified from Orsi et al., 1999); b) location map (Google Earth); c) cross section corresponding to the black line (X–X′) in (a) (Orsi et al., 1996). (For interpretation of the references to colour in this figure legend, the reader is referred to the web version of this article.)

Neapolitan Yellow Tuff (14.9 ka, Orsi et al., 1992, 1996, 2004; Wohletz et al., 1995; Deino et al., 2004). The third period is characterised by a series of magmatic and phreatomagmatic events, mainly confined to the north-eastern sector of the Neapolitan Yellow Tuff caldera and potentially related to tectonically controlled localised upwelling (Isaia et al., 2009; Arienzo et al., 2010). The last eruption in historical time is the 1538 Mt. Nuovo eruption (Di Vito et al., 1987); 400 years of quiescence have been interrupted by two periods of bradyseism (1969–72 and 1982–84) which lead to 3.5 m of total vertical deformation (Troise et al., 2008). Slow subsidence interrupted by short uplift events characterises the current deformation pattern of the caldera (De Martino et al., 2014).

Many conceptual models have been proposed to explain the high level of activity of Campi Flegrei and in the last couple of decades there has been consensus that caldera deflation periods can be explained by the relationship between poro-elastic properties of the caldera fill and fluid flow (e.g., Bonafede, 1991; Orsi et al., 1999; De Natale et al., 2001; Battaglia et al., 2006). The impact of hydrothermal fluid circulation on rock mechanics provides a minor contribution to uplift phases (Rinaldi et al., 2011; Coco et al., submitted for publication). The model proposed by Bodnar et al. (2007) suggests an intermittent mechanism able to provide fluids (mainly gas) to the shallow hydrothermal reservoir. The deep cooling and degassing magma body provides fluids which are kept at depth, trapped around the magma body, until rock failure allows their release. These fluids then migrate towards the surface inducing deformation; contrastingly, degassing allows deflation.

In the last 45 years, following the 1970 bradyseism crisis, an impressive monitoring effort developed in the Neapolitan region, including continuous recording of ground deformation, seismicity and degassing (since 1998), as well as large scale tomography campaigns (Vanorio et al., 2005; Zollo et al., 2008; De Siena et al., 2010; Capuano et al., 2013) and, more recently, high resolution resistivity studies (Bruno et al., 2007) to constrain the geometry of the subsurface structures. The ongoing activity of the area and the abundance and variety of data collected by the widespread monitoring network have progressively changed and improved our understanding of the system.

Most of the early interpretation of ground deformation considered the source of uplift to be a pressure and volume change within the magma chamber (Bonafede et al., 1986; Berrino, 1994). However, a very shallow (<3 km) pressure source seems to be required to fit the observed ground deformation data (Bonafede, 1991; Gottsmann et al., 2006; Amoruso et al., 2008), unless structural discontinuities (Acocella et al., 1999) localise the deformation induced by pressure or volume changes in the deep magma chamber (De Natale and Pingue, 1993; Orsi et al., 1996, 1999; De Natale et al., 1997; Acocella et al., 2000; Folch and Gottsmann, 2006). Prior models that supported the coupling of magmatic and hydrothermal interaction during unrest crises (e.g., Gaeta et al., 1998; De Natale et al., 2001; Battaglia et al., 2006) pointed out the role of hydrothermal fluid flow in dissipating ground inflation, especially in the absence of a volcanic eruption after inflation.

Although the primary source of gas seems to be a deep-seated (>2.5 km) gaseous reservoir (Chiodini and Marini, 1998; Chiodini et al., 2001, 2012), additional shallower gas-rich pockets have been inferred, based on thermometric data (Caliro et al., 2007) and an electrical resistivity campaign (Bruno et al., 2007). Water-saturated rocks and aquifers have also been identified during the drilling of the AGIP-ENEL geothermal wells (1939–1979). In particular, in the fractured rocks of the Mofete area (Fig. 1), aquifers occur at 550–1500 m, 1900 m and 2700 m (Carella and Guglielminetti, 1983), defining the hydrothermal reservoir as the multiphase shallower portion of a complex vertical succession of reservoirs. However the mechanism and relative importance of advection and diffusion of gas, water and heat are still unclear. Furthermore Townend and Zoback (2000) suggest that critically stressed faults, as Campi Flegrei faults seem to be during uplift (Troise et al.,

1997), are hydraulically highly conductive. Therefore faults likely play an important role in fluid flow and energy transport.

The extensional Upper Pliocene tectonism that initiated magmatism in the area led to the development of two major structural discontinuities parallel and perpendicular to the Apennine trend. The approximately rectangular area marked by those structures is the most seismically and geodetically active (Orsi et al., 1999). Superimposed on these tectonic alignments are linear faults and fractures formed by brittle deformation in response to volcanic activity, including ring faults from caldera collapse and faults around the crater rims of the monogenic volcanic centres. An example of this brittle response is the NE–SW fracture formed within the Solfatara crater after the 1982–1984 bradyseism (Acocella et al., 1999) and the intensely fractured zone, with high rates of diffuse degassing, between the fumarolic areas of Solfatara and Pisciarelli (Chiodini et al., 2010). According to structural models (Rubin, 1995; Troise et al., 1997; Acocella et al., 1999; Saunders, 2004) ring faults facilitate the emplacement of magma but, because the initial stage of many volcanic eruptions at Campi Flegrei were phreatomagmatic (Newhall and Dzurisin, 1988; Guidoboni and Ciuccarelli, 2011), it seems likely that faults also localise aqueous fluid flow. The ground deformation dynamics characterised by rapid uplift phases and slow relaxation (Dvorak and Mastrolorenzo, 1991), as well as the extensive hydrothermal activity inside the caldera, suggest an important role of ground water and fluid flow in recent unrest.

3. Method

Our simulations implement the TOUGH2 code (Pruess et al., 1999) which has been previously used for numerical simulations of flow within Campi Flegrei caldera (Chiodini et al., 2003, 2010; Todesco et al., 2003, 2004, 2010; Todesco and Berrino, 2005; Rinaldi et al., 2010, 2011; Petrillo et al., 2013). TOUGH2 solves mass and energy balance equations that describe fluid flow and heat transport in multiphase, multicomponent systems. For each grid block, the primary thermodynamic variables (P, T, pCO$_2$) as well as all the other thermophysical parameters (phase saturation, relative permeability, viscosity, density, specific enthalpy, capillary pressure, diffusion factors and mass fractions) are computed to solve the governing flow and transport equations as function of time. The description of thermodynamic conditions is based on the assumption of local equilibrium of all phases. The basic equation of the code is a multiphase extension of Darcy's law; heat is transported by conduction and convection, including sensible as well as latent heat effects. Detail formulation of the equations can be found in Pruess et al. (1999).

Based on to the simulations of Todesco et al. (2010) of the shallow (<1.5 km depth) hydrothermal reservoir of Campi Flegrei caldera, we specify a 2D axisymmetric (radial grid, Fig. 2a) slice extending 10 km from the centre of the caldera to beyond the caldera rim. The space is discretised to 3315 grid blocks of 100 m thickness and with radial dimension ranging from 20 to 200 m, allowing higher resolution close to the fumarole and faults, after Todesco et al. (2004, 2010). The model is initially water saturated. The model is initially water saturated, with an open boundary at the top fixed at atmospheric pressure and temperature of 20.5 °C, which simulates the water table. The lateral boundaries are impermeable and adiabatic whilst the basal boundary behaves, in most of the simulations, as a heat source. Todesco et al. (2010) assume an initial conductive temperature profile; here we introduce a constant basal heat flux (0.2 W/m^2) able to sustain the local geothermal gradient (100–170 °C/km, Rosi and Sbrana, 1987; Piochi et al., 2014; De Siena et al., 2010; Carlino et al., 2012), which has not been considered in previous Campi Flegrei models. Initial temperature and pressure are defined as functions of depth following an average geothermal gradient of 130 °C/km and assuming hydrostatic conditions. The depth of the 400 isotherm that approximately marks the brittle/ductile transition (Fournier, 1999), is at about 3 km, consistent with the assumption of hydrostatic conditions for the depths of our simulation domain.
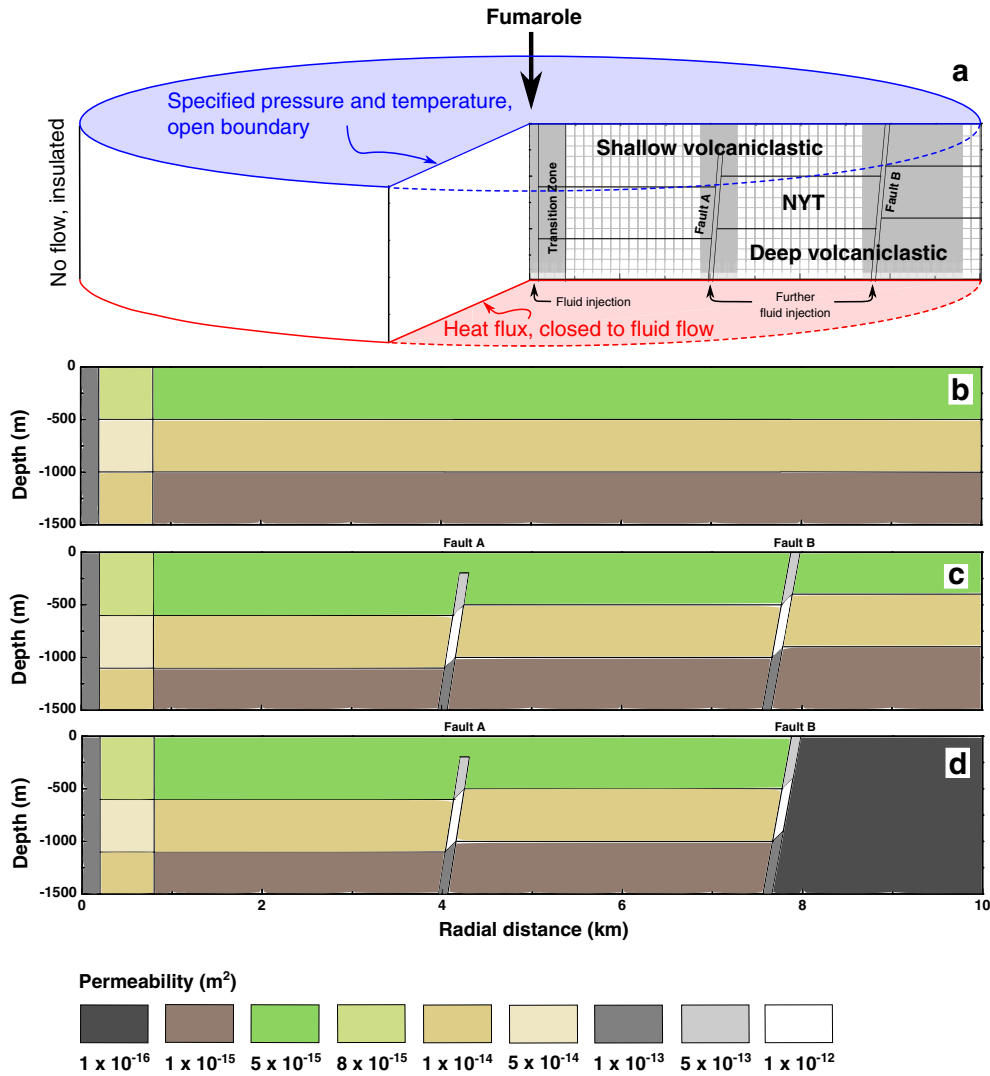
Fig. 2. Simulation grid and boundary conditions (a) and distribution of permeabilities in three contrasting geometries: b) baseline model geometry after Todesco et al. (2010); c) introduction of two steep faults and relative offset (100 m), this geometry is our reference model; d) lithological contrast on the right side of the model, simulating the effect of the caldera margin.

High enthalpy fluids, representing the magmatic fluids that feed the Campi Flegrei caldera fumaroles, are injected into the basal cells over a radial distance of 200 m. Following the previous models of Todesco et al. (2004, 2010), constrained by gas chemistry measurements (Chiodini et al., 2001, 2003, 2010), we inject 1000 t/day of CO_2 and 2400 t/day of H_2O at enthalpies of 2.98×10^6 J/kg and 1.15×10^5 J/kg, corresponding to a fluid temperature of 350 °C (Todesco et al., 2010). After the injection of this high enthalpy fluid, a gas rich-phase develops at the centre of the Campi Flegrei caldera, which has been interpreted as the reservoir feeding the fumaroles.

Table 1
Reference model rock properties.

	Permeability (m²)	Porosity	Thermal conductivity (W m⁻¹ K⁻¹)	Specific heat (J kg⁻¹ K⁻¹)	Density (kg m⁻³)
Fumarole	1×10^{-13}	0.1	1.15	900	1800
Transition zone near fumarole					
Volcanic and marine sediments < 12 ka	8×10^{-15}	0.15	1.15	900	1600
NYT	5×10^{-14}	0.15	1.15	900	1800
Volcanic and marine sediments 12–39 ka	1×10^{-14}	0.15	1.5	1000	2000
Caldera fill					
Volcanic and marine sediments < 12 ka	5×10^{-15}	0.45	1.15	900	1600
NYT	1×10^{-14}	0.35	1.15	900	1800
Volcanic and marine sediments 12–39 ka	1×10^{-15}	0.15	1.5	1000	2000
Faults					
Volcanic and marine sediments < 12 ka	5×10^{-13}	0.45	1.15	900	1600
NYT	1×10^{-12}	0.35	1.15	900	1800
Volcanic and marine sediments 12–39 ka	1×10^{-13}	0.15	1.5	1000	2000

Relative permeability follows the Corey's curve with residual gas fraction of 0.05 and residual water saturation of 0.3. Capillary pressure increases linearly with liquid saturation.

The conceptual and numerical models of Campi Flegrei have evolved over the last decade (Chiodini et al., 2003; Todesco et al., 2003, 2004, 2010; Piochi et al., 2014). Here, as in Todesco et al. (2010), we simulate a layered system where 500 m thickness of volcanic and marine sediments (<12 ka) overlies the 500 m thick Neapolitan Yellow Tuff (NYT), below which is a 500 m thickness of volcanic and marine deposits (12–39 ka) emplaced following the earlier Campanian Ignimbrite caldera collapse. Hydraulic properties (permeability, porosity, thermal conductivity, specific heat and rock density) of the caldera fill, as well as relative permeability and capillary pressure, are constrained by published values from cored wells and the fit of prior models which in turn were constrained by observations of ground deformation and gas chemistry (Table 1, Fig. 2). Permeability is initially assumed to be isotropic and is highest in the Neapolitan Yellow Tuff (10^{-14} m^2), whilst older volcanic and marine sediments are less permeable (10^{-15} m^2), lower than younger equivalents overlying to Neapolitan Yellow Tuff (5×10^{-15} m^2), reflecting the effect of compaction. The zone of diffuse degassing in the Solfatara–Pisciarelli area has been simulated as a high permeability (10^{-13} m^2) conduit of 200 m radius, corresponding to the radius of the Solfatara crater. The zone of contact ("transition") between the conduit feeding Solfatara and the caldera fill (extended to 800 m radius) is assigned properties intermediate between the conduit and the remaining caldera fill to represent the effect of the network of fractures (Table 1, Fig. 2).

In contrast to previous work, our simulations incorporate the steep-angled normal faults (60–70°) that characteristically dissect the Campi Flegrei caldera (Orsi et al., 1996; Chiodini et al., 2001; Bruno et al., 2007). According to Orsi et al. (1996) (Fig. 1c) some faults outcrop to the surface whereas other are buried by the recent volcanic and marine sediments. We include dip angle, lithological offset and different vertical extent of the faults. Two faults (A and B) are defined either as high permeability structures (100 m wide) to simulate open and active faults and the associated highly fractured damage zones, or as lower permeability discontinuities within the shallow hydrothermal reservoir to simulate the effect of sealing by fault gauge and mineral precipitation.

Our reference case includes vertical permeability (k_v) in the fault zone two orders of magnitude higher than in the caldera fill adjacent to the faults. In further simulations to illustrate the influence of fault permeability, k_v in the fault zone is adjusted relative to the host rock by factors ranging from 10^2 to 10^{-4} times the reference case values. Fault A is located at 4 km from the central axis with a minor (100 m) offset in the caldera fill. The top of fault A terminates at 200 m depth, whereas fault B crosscuts the entire domain at a distance of 7.5 km from the centre of the fumarole, representing a major discontinuity in the system. Fault A delineates the caldera ring fault associated with the NYT caldera collapse, whereas fault B can be visualized either as the contact between the Neapolitan Yellow Tuff caldera and Campanian Ignimbrite deposits (with fault offset 200 m), or as the outer edge of the Campi Flegrei caldera (Fig. 2d), following the model of the nested and resurgent caldera of Orsi et al. (1996). In our model of the latter case, we assume that the domain outside of fault B has low permeability (10^{-16} m^2) and we set the specific heat to 1000 J/kg K by analogy with the younger products. We also evaluate the role of permeability anisotropy of the caldera fill by increasing the horizontal permeability one and two orders of magnitude with respect to the vertical.

Table 2A, B summarises the experimental design and relationship between simulations used to evaluate the role of faults and their interactions with caldera fill deposits. We begin by simulating the hydrothermal system at Campi Flegrei during a period of quiescence and examine the nature of fluid flow and heat at steady state. To the initial simulation, based on the heterogeneous simulations described

Table 2
Simulated parameters. Simulations of unrest are based on our reference model (model 2).

A. Model development

Simulation number	Figure	Fault-k_v relative to caldera fill-k	Basal heat (W/m^2)	Fluid injection at faults[a]		
				CO$_2$ (td^{-1})	H$_2$O (td^{-1})	CO$_2$/H$_2$O (molar ratio)
1—Baseline (based on Todesco et al., 2010)	Fig. 3		0.2			
2—Reference	Figs. 4, 5	100	0.2			
3—Fluid injection	Fig. 6	100	0.2	1000	2400	0.17

B. Sensitivity analysis

Simulation number	Figure	Fault-k_v relative to reference	Basal heat (W/m^2)	Caldera fill-k_h relative to reference	Lithological contrast
4—Ref. × 0.1 fault k_v		0.1	0.2	1	
5—Ref. × 10 fault k_v	Fig. 7	10	0.2	1	
6—Ref. × 100 fault k_v		100	0.2	1	
7—Ref. × 10 caldera fill k_h	Fig. 8	1	0.2	10	
8—Ref. × 100 caldera fill k_h	Fig. 9	1	0.2	100	
9—Lithological offset	Fig. 10	1	0.2	1	✓[b]

C. Simulation of unrest

Simulation number	Figure	Basal heat (W/m^2)	Fluid injection at faults[a]		
			CO$_2$ (Td^{-1})	H$_2$O (Td^{-1})	CO$_2$/H$_2$O (molar ratio)
10—Unrest at faults: quiet		0.2	1000	2400	0.17
11—Unrest at fumarole & faults: crisis	Figs. 11, 14	0.2	6000	6100	0.40
12—Increased basal heat flux	Figs. 12, 13, 15	10			

[a] See Todesco et al. (2010, Table 1 — Quiet and Crisis) for input parameters. Fluid composition and flux into the fumarole are the same for all the simulations except model 11.

[b] See Fig. 2d.
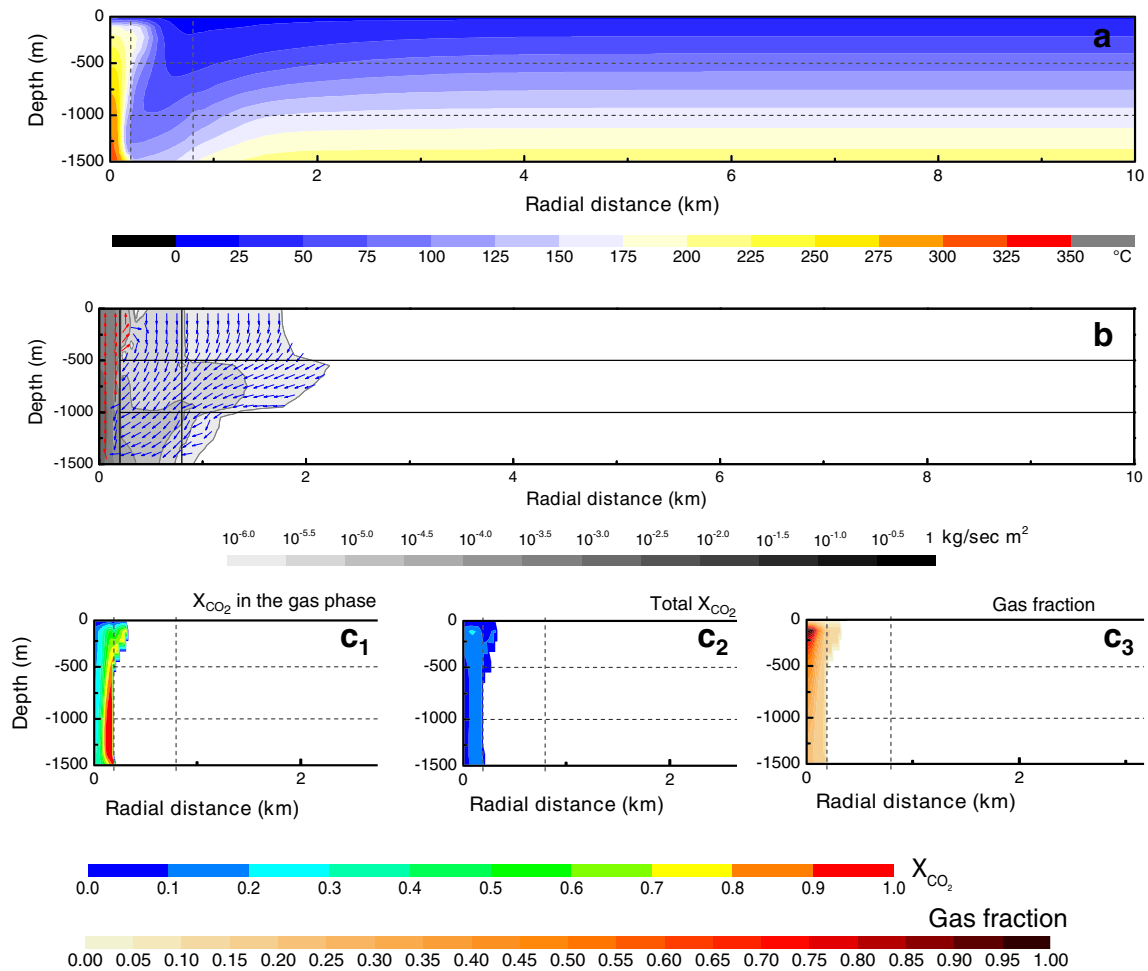
Fig. 3. Baseline model (model 1): a) temperature distribution at steady state showing 200 m radius fumarolic plume at the caldera centre; b) magnitude of fluid flow in kg/s m^2 (background colours) and vectors representing flow direction (red-upward flow and blue-downward flow), the threshold for displaying flow is arbitrarily fixed at 10^{-6} kg/s m^2; c1) CO_2 fraction in the gas phase; c2) CO_2 fraction in the fumarole as sum of CO_2 gas and CO_2 dissolved in water; c3) gas fraction. (For interpretation of the references to colour in this figure legend, the reader is referred to the web version of this article.)

in Todesco et al. (2010), we assign a conductive heat flux across the entire base of the model (model 1, baseline model) and we add two high-transmissivity faults (model 2, reference model). We also investigate the connectivity of faults with the deep gas-rich reservoir that feeds the fumarole (model 3), with the fluid injection set equal to the mass flow rate and composition of injected fluids during quiet "periods" as in Todesco et al. (2010). We ran the simulation for 4000 years; however, in this scenario steady state is not reached.

From our reference model (model 2) incorporating permeable faults and basal heat flux, we evaluate the sensitivity of fluid flux and temperature to key parameters: i) the permeability of the faults (models 4–6), ii) anisotropy (k_v/k_h) of the caldera fill (models 7 and 8), and iii) the existence of contrasting lithologies at the caldera margin (fault B, model 9).

We also ran three models (simulations 10–12) to simulate volcanic unrest, where the steady state reference model (model 2) is perturbed by changing the fluid flux or basal heat flux conditions (Table 2C). We compare the response time of the system to the perturbations, running simulations sufficiently long to observe significant changes in the surface temperature or fluid pressure (which could be manifest in nature as ground deformation). In the first unrest scenario (model 10) fluid is forced into the fumarole and both faults, using the fluid flux and fluid chemistry of model 3. However the initial condition is not the uniform temperature gradient of 130 °C/km as in model 3, but the steady state condition of the reference model. For model 11, the flux of hot water and CO_2 at the fumarole and faults is increased by a factor 3.6 and the CO_2/H_2O molar ratio is increased by a factor of 2.4, relative to model

10. These fluid parameters are based on the mass flow rate and composition of injected fluids during a "crisis" in Todesco et al. (2010). The third unrest scenario (model 12) aims to simulate perturbation of the deeper portion of the Campi Flegrei caldera and its effect on the shallow hydrothermal system. We therefore increase the heat flux at the base of the model by two orders of magnitude (to 10 W/m^2) compared to the steady state condition. Models 10 and 11 simulate unrest dominated by forced convection of hot fluids whereas in model 12 unrest is dominated by an increase in conductive heat input.

4. Results

4.1. Model development

Results for the baseline simulation, lacking faults, are presented in Fig. 3 and reproduce all the main features shown by Todesco et al. (2010). A steady state convective flow system develops within 4 ky in which the injection of 3400 T/day of hot (350 °C) H_2O–CO_2 fluids feeds a narrow plume, the radius of which increases from 150 m at −1500 m to 225 m at the top of the model, where temperatures reach a maximum of 180 °C (Fig. 3a), which is comparable with the 150 °C (Vaselli et al., 2011) measured at Solfatara. The total fluid flux within this plume is substantially greater than that injected due to entrainment of water from the surrounding aquifer. This aquifer water component is sourced from downward flow from the top of the model domain at mean annual temperature. Significant cooling occurs in the
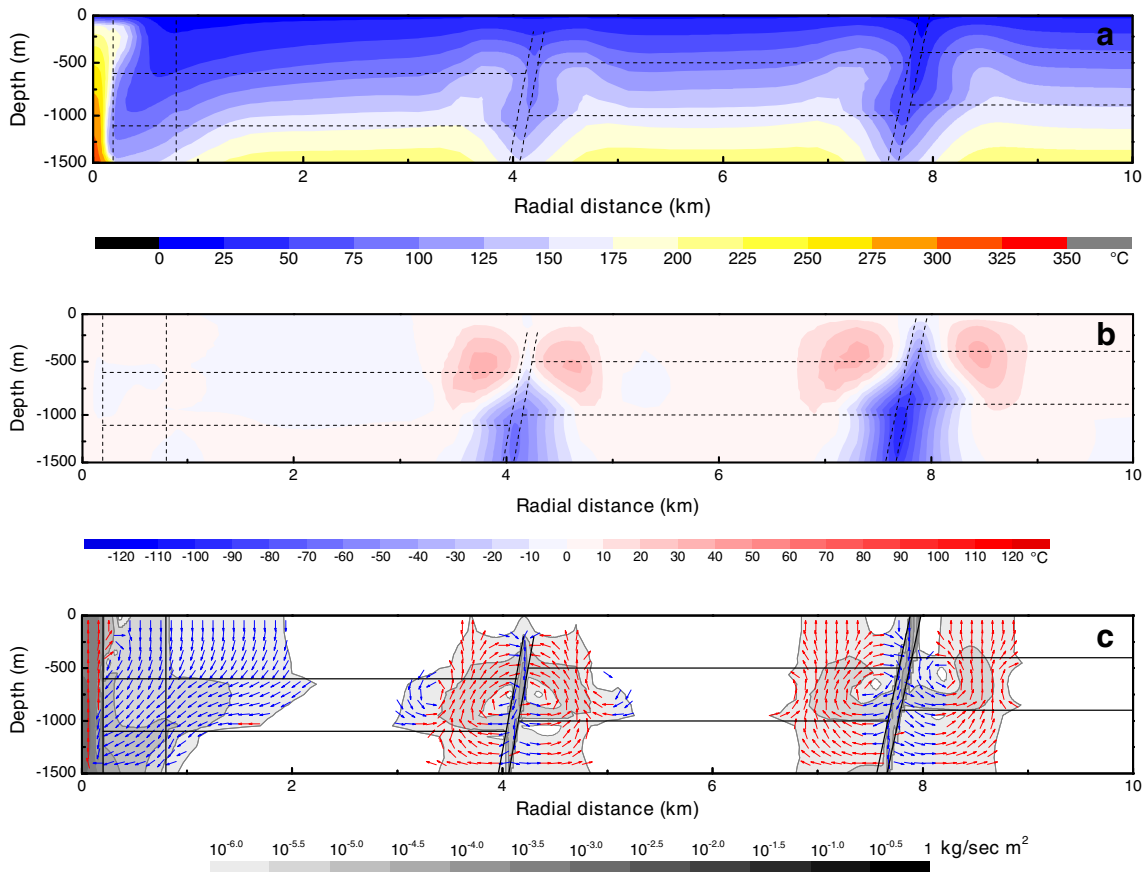
Fig. 4. Reference model (model 2) at steady state: a) temperature distribution shows fault zones are the cooler portion of the reservoir; b) temperature difference between reference model and baseline model, showing a temperature drop up to 90 °C on faults and high temperature anomaly up to 30 °C at 500 m depth; c) flow field (see Fig. 3b for plotting details). Three separate advective domains (fumarole, fault A and fault B) develop after the introduction of two steep faults at 4 and 7.5 km from the fumarole. Faults enhance the cooler groundwater recharge of the hydrothermal system.

downward limb of the advection cell, with depression of the isotherms by up to 500 m in the zone 400–1500 m from fumarole. Negligible fluid flow ($<10^{-6}$ kg/s m^2) occurs in the more distal parts of the system (>2 km from the fumarole, Fig. 3b) where temperature and pressure gradients average around 0.13 °C/m and 0.01 MPa/m respectively.
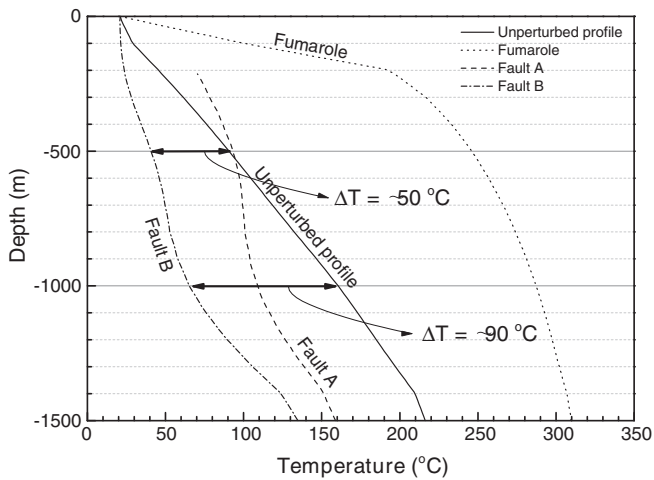

Fig. 5. Vertical temperature profile of reference model (model 2) at the fumarole, fault A, fault B and the unperturbed temperature gradient far from the faults (6 km radial distance from the fumarole). Cooling due to ground water recharge is shown at both faults, with a maximum temperature drop of 90 °C at fault B.

The forced convection system involves a mixture of injected gas, relatively low density hot water, and denser cold aquifer water. The injected gas, moves upwards developing a 400 m radius fumarolic plume: a two-phase mixture of gas and liquid of two components (H_2O and CO_2). Over the ranges of temperature and pressure of the plume, CO_2 is either dissolved into the liquid phase or transported in the gas phase. At high gas saturation the system is steam dominated, whereas at low gas saturation, at the cooler edge of the plume, the amount of steam drops leading to a relative enrichment in CO_2 (Fig. 3c). The effect of CO_2 on the density of the liquid phase is negligible ($<6\%$ by mass). In contrast the presence of CO_2 has a significant effect on the total fluid (liquid + gas) density, especially at low gas saturation where CO_2 (not H_2O vapour) is the dominant gas component. The presence of gas (either CO_2 or H_2O) in the fumarolic plume leads to a drop in total fluid density of 20%. In the absence of gas, beyond 400 m from the fumarole, liquid density is controlled solely by temperature.

The introduction of basal heat flux does not significantly affect either the flow pattern or the average temperature gradient, which at radial distance > 2 km from the fumarole increases from about 0.10 °C/m (without basal heat flux, as determined by Todesco et al., 2004) to 0.13 °C/m (model 1). The limited effect of basal heat flux is due to the thermal equilibrium reached between the injection of hot fluids, cold groundwater recharge and the initial temperature gradient imposed on the domain that takes into account the high heat flux at Campi Flegrei.

The introduction of steep faults (model 2) allows recharge of cold shallow groundwater into the reservoir with upwelling of warmer waters within a zone extended 500 m either side of the faults (Fig. 4a, c). At
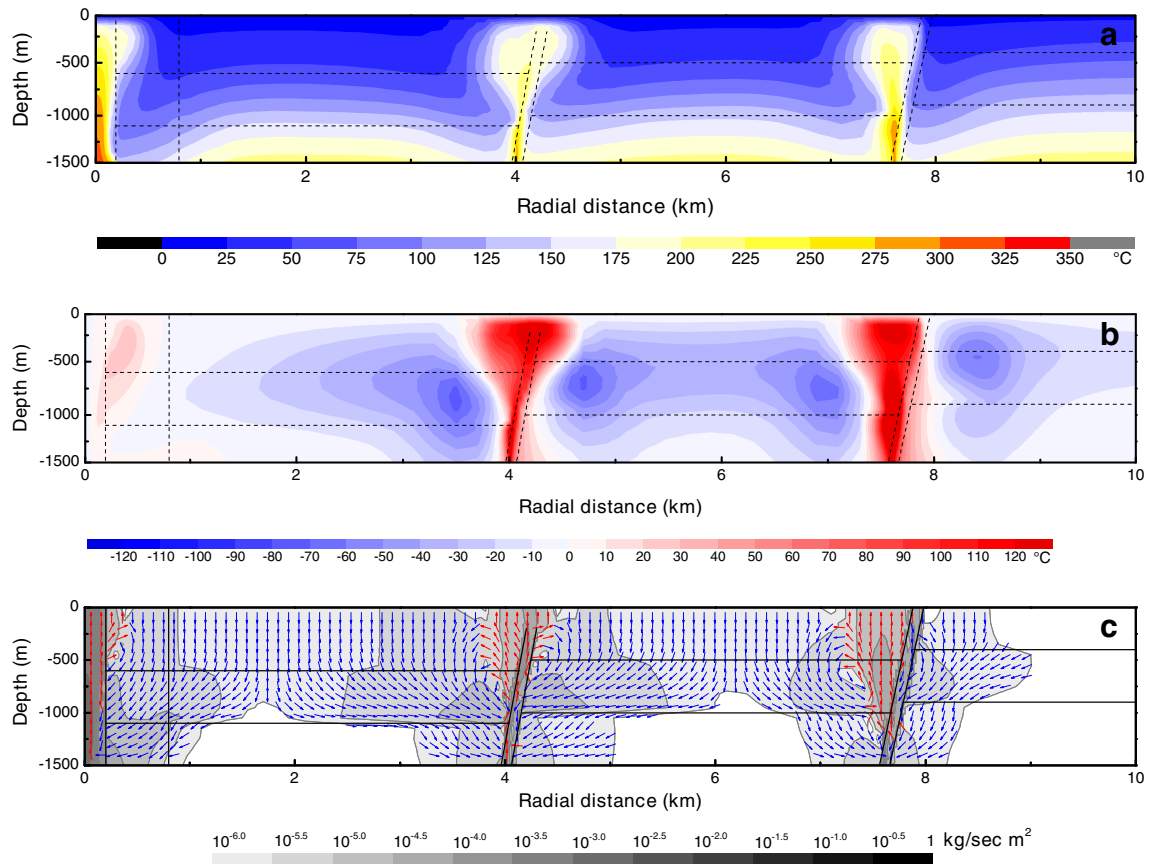
Fig. 6. Model 3 results at steady state: a) temperature distribution after 4 ka of injection of fluids at faults as well as fumarole, showing the development of hot plumes with anisotropy on fault B; b) temperature difference between model 3 and the reference model (model 2): hot plumes develop on faults however, between injection points, the system is cooler than the reference by up to 60 °C because of the higher recharge rate; c) flow field (see Fig. 3b for plotting details). Three convective cells develop with flow divides at 2 and 6 km. Fault A discharges fluids at the surface after recharge from both sides of the fault whereas on fault B recharge preferentially occurs along the fault zone and on the footwall, with preferential discharge on the hanging wall.

the base of the shallow volcaniclastic unit, waters are up to ~40 °C warmer than in the baseline model (without faults, model 1), whilst at the base of the Neapolitan Yellow Tuff the system is cooler by up to 90 °C (Fig. 4b). The cooling effect at fault B, which crosscuts the whole domain, is 34 ± 12 °C (average ± 1σ) greater than that at fault A which terminates 200 m below the surface. The stratification offset across faults leads to slightly greater cooling at 950 m on the footwall of fault B.

Advection associated with groundwater recharge causes cooler temperatures along faults (Fig. 5). Although the fumarolic circulation system and the circulation cells developed at faults are separated by a flow divide at about 2 km radial distance, the presence of faults radially extends the fumarole recharge zone by about 100 m (compare Fig. 3b and Fig. 4c). The zone where temperature is perturbed by the presence of faults lies beyond the fumarolic circulation system (>2 km, Fig. 4b).

Depending on the depth to which the permeable fault zones extend and their connectivity with deeper high enthalpy fluids, they could be influenced by input from the hydrothermal reservoir, which also feeds the fumarole. Injecting fluids at the base of faults A and B (model 3), leads to the development of hot plumes around both faults with concomitant sharp lateral temperature gradients of 0.30 °C/m at 250 m depth on both sides of the hot fluid advective plumes (Fig. 6a). In both fault systems discharge is favoured in the hanging wall reflecting the offset in stratigraphically controlled caldera fill permeability. However where the fault extends to the top of the model domain (fault B) the upwelling plume diverges from the fault zone at depth and the upper part of fault B becomes a conduit for recharge. This advective cell recharges within the footwall of fault B and brings high temperature fluids

(up to 140 °C) towards the surface. Volumes of fluid drawn into the system from the top of the model are significantly greater than in the reference model, with most lateral flow around the fault zones within the Neapolitan Yellow Tuff. The strong forced convection that develops around fault A diverts 60% of the horizontal groundwater flow component from the fumarole towards fault A, reducing the cooling power of groundwater recharge on fumarolic fluids and increasing the temperature at the edge of the fumarolic plume by ~20 °C (Fig. 6b, c).

4.2. Sensitivity analysis

4.2.1. Fault permeability

In the reference simulation (model 2) vertical permeability in the fault zones is two orders of magnitude higher than in the caldera fill. We present a series of simulations in which we investigate the impact of different fault permeability values, keeping initial and boundary conditions the same as model 2. With fault zone vertical permeability only one order of magnitude higher than the caldera fill (model 4) the impact of faults on both heat and fluid fluxes is negligible and simulations (results not shown) resemble the base case.

However, increasing the permeability contrast between faults and the caldera fill to three and four orders of magnitude (models 5 and 6) changes the behaviour of the flow system (Fig. 7a). The cooling effect of descending shallow fluids is enhanced relative to the reference model. For a three order of magnitude permeability contrast (model 5) expansion of zones of cooling (greatest in the Neapolitan Yellow Tuff) and warming (greatest in the shallow volcaniclastics) occurs around fault B. Fault A switches from being a focus for cool water
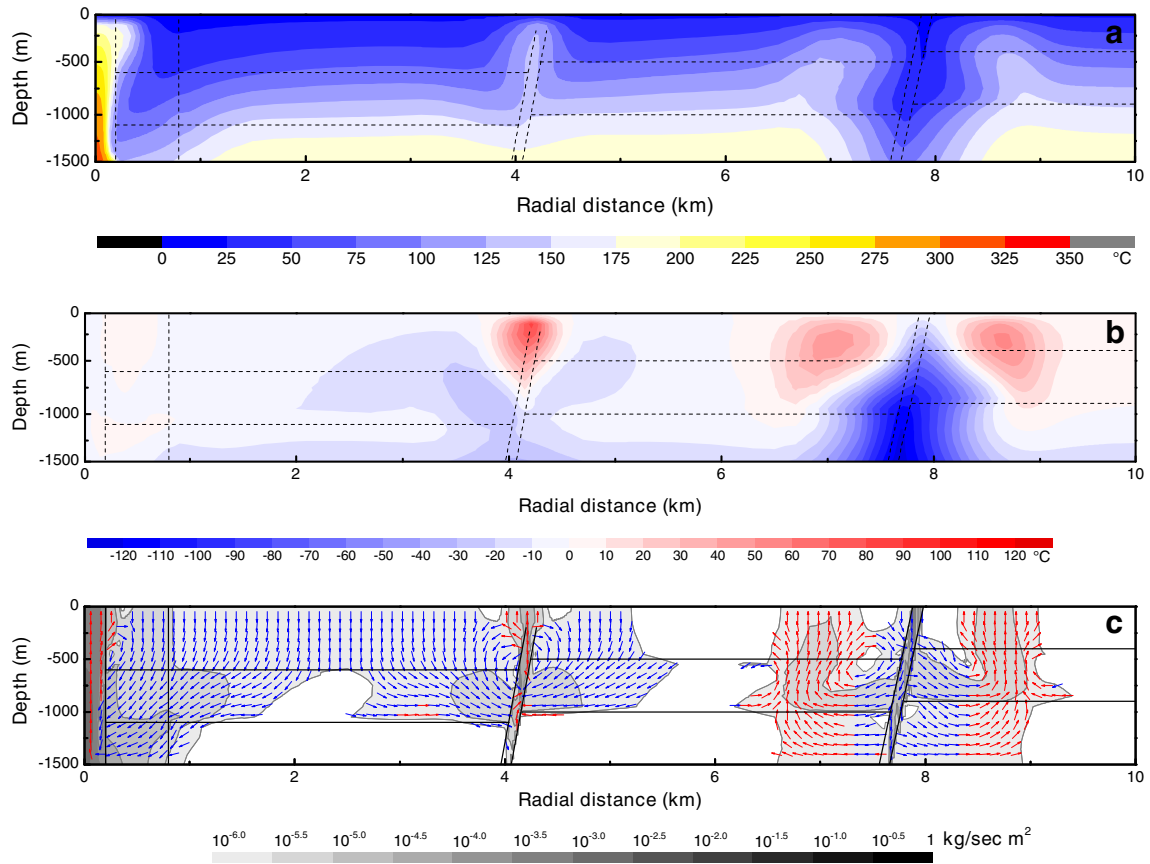
Fig. 7. Model 5 (steady state): increasing permeability contrast between faults and caldera fill by one order of magnitude inverts the direction of flow at fault A. a) Temperature distribution: at fault A a temperature gradient of 0.60 °C/m occurs over the first 200 m depth, then temperature is almost constant at 130 °C to 750 m depth. b) Temperature difference between model 5 and the baseline model (model 1): groundwater cooling at fault B approaches 100 °C at 1.5 km depth, conversely the maximum increase of temperature (80 °C) occurs near the top of fault A. c) Flow field (see Fig. 3b for plotting details): groundwater flow extends within most of the shallow volcaniclastic deposit and the Neapolitan Yellow Tuff, fluid discharge occurs at fumarole and fault A, whilst recharge and advective upwelling occur at fault B.

recharge to a zone of discharge of warm waters, up to 60 °C warmer than ambient temperature (Fig. 7b). With upward flow in fault A, the zone of significant ($>10^{-6}$ kg/s m^2) downward flow at shallow depth extends from the fumarole to fault A (Fig. 7c). The focused downflow in and around fault B results in cooling relative to the baseline model (Fig. 7b). Further increase of fault permeability (model 6) makes negligible differences in results (not shown), because the flow rates are limited by the permeability of the caldera fill.

4.2.2. Permeability of the caldera fill

Horizontal permeability (k_h) of caldera fill may be higher than vertical permeability because of depositional layering and/or compaction and welding (Peluso and Arienzo, 2007; Wright and Cashman, 2014). Our simulations show that increasing the horizontal permeability of the caldera fill by one and two orders of magnitude (models 7 and 8, respectively) allows not only significant flow of fluids throughout the domain, but also enhances mixing between deep and superficial fluids.

The effect of a one order of magnitude increase in caldera-fill k_h, is clearly shown by the distribution of temperature (Fig. 8a, b); the temperature of the fumarolic plume is only slightly reduced but the volume-averaged temperature of the caldera drops from 119 °C in the reference model to 109 °C. Not only are lateral temperature contrasts enhanced significantly, but the stratigraphic contrasts in permeability have a clearer impact. Fault B, continues to function as a recharge zone with upwelling of warm water extending 2 km either side. Fluids also flow downward in fault A in the lower volcaniclastic unit. However fault geometry and lithological offset result in discharge both within the fault zone and in the hanging wall in the upper part of the stratigraphy, fed by recharge through the footwall. The effect of the juxtaposition

of different lithologies and the displacement by faults are highlighted by the higher fluid flow rates.

Increasing the caldera fill horizontal permeability further (model 8), by two orders of magnitude relative to reference model, reduces the width of the zone contributing to the fumarole. The central portion of the domain shows a 2 km radius convection cell, where fault B is the downward limb of the convection cell and fault A the upward one (Fig. 9c). The elevated k_h drives significant overall cooling with a volume-averaged temperature ~20 °C lower than the reference model. Cooling is marked within the Neapolitan Yellow Tuff and underlying volcaniclastics, whilst enhanced vertical advection warms much of the upper volcaniclastic unit (Fig. 9a, b).

In the context of the nested resurgent caldera of Campi Flegrei, we evaluate the effect of a strong lithological contrast on fluid flow at the caldera margin by interpreting fault B as the caldera ring fault. Setting permeability outside the caldera to 10^{-16} m^2 (model 9, Fig. 2d) forces fluid discharge through fault B (which is a recharge zone in the reference model) and drives recharge to the hanging wall (Fig. 10c). Accordingly temperatures are elevated along fault B (Fig. 10a) reaching 62 °C at 150 m depth compared to 36 °C in the adjacent footwall. The combination of cooling along fault B in the reference model and up-welling of hot fluids in model 9 produce a maximum temperature difference between these two simulations of 94 °C (Fig. 10b).

4.3. Unrest

The following models evaluate the temporal evolution of the caldera during three possible unrest scenarios. The initial condition of the unrest scenarios is the steady state condition of the reference model
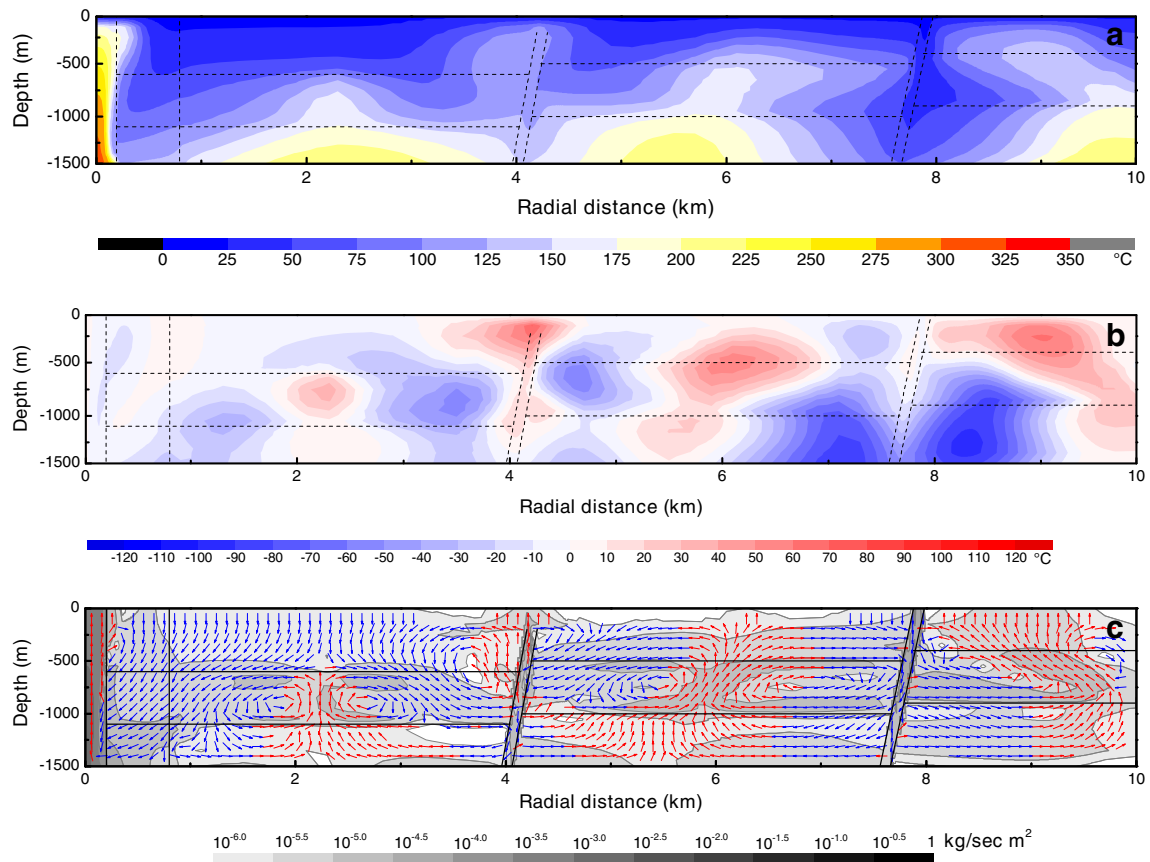
Fig. 8. Model 7 steady state results with one order of magnitude increase in caldera fill k_h: a) the temperature distribution; b) the system is cooler with respect to the reference model, with localised advection-driven high-temperature anomalies; c) significant ($>10^{-6}$ kg/s m^2) fluid flow extends to the whole caldera, however flow divides still occur at 2 km and 6 km.

(model 2) that we then perturb by injection of high enthalpy fluids at two different rates and chemistries ("quiet" and "crisis" conditions of Todesco et al. (2010)) or by increasing basal heat flux (Table 2C). We present the temporal evolution of the system, which is important for interpreting unrest conditions.

The results of fluid injection simulations with different fluxes and chemistries (model 10 and 11) are almost identical except for the time needed for the injected fluids to reach the surface (using temperature as a tracer of advection) and the lack of widening of the fumarolic plume in the quiet rate scenario (model 10; results not shown). High enthalpy fluids injected at the base of the fumarole and faults migrate upwards, leading to a maximum temperature of 180 °C near the surface. As in model 3 (which has the same fluid input and permeability structure as model 10), the maximum temperature occurs above the fluid injection point, with significant lateral offset from the top of fault B (Fig. 11b, c). The injection of mass (fluids) within the reservoir initially forces upward flow within the entire caldera; however, whilst the high temperature front moves upwards, the cooler groundwater component entrained in the plume increases, allowing the development of double convection systems centred on the faults. On fault B the convective cell develops at depth greater than 500 m governed by the permeability contrast between the Neapolitan Yellow Tuff and the Shallow Volcaniclastics (Fig. 11). The dominant upflow changes into convective flow when the hot fluids reach the surface, which takes 300 years of injection in the quiet rate scenario and 100 years in the crisis rate scenario. The higher flux at the fumarole relative to all the other simulations leads to a widening of the fumarolic plume of about 200 m at the top of the plume.

The last unrest scenario, model 12, evaluates the impact of a sudden one order of magnitude increase in basal heat flux on the hydrothermal

reservoir. Fig. 12 shows the temperature, fluid flux and the fluid pressure change with respect to the initial condition at 100 (a), 110 (b) and 120 (c) years after the introduction of higher heat flux. The coupling of gas formation at depth and cooler water influx generates a 32 ± 5 year discharge/recharge cycle, comprising alternating phases of (A) upward and (B) downward flow of groundwater (Fig. 13). The system heats up initially at points most distant from the cooling influence of the faults (2 km, 6 km and 9 km distance from the fumarole) (Fig. 12a$_1$–c$_1$). The heating causes boiling in basal zones between the faults. Cooling during fluid ascent results in condensation and limits the development of these gas-rich pockets to depths > 1300 m. Over time the boiling front moves laterally towards the faults. For example, the outer margin of a boiling zone between faults A and B extends from 7000 m to 7300 m radial distance at 1500 m depth over a period of 20 years (Fig. 12a$_3$–c$_3$). The proximity of fault B to the closed outermost boundary advances the development of gas on the outer portion of the domain (>8 km from fumarole) by about 5 years compared to the zones at 2 km or 6 km (Fig. 12c$_3$).

An example of the record of cycling is presented in Fig. 13, which shows temperature, pressure, vertical fluxes and gas fraction time series for a point at 1500 m depth and 5900 m distance from the fumarole (point P$_1$ in Fig. 12). Temperature initially increases approximately linearly (at an average of 1.24 °C/year) as a result of the elevated heat flux until, after 90 years, the boiling point is reached (Fig. 13a). This leads to production of gas and increased fluid pressure, which before boiling had remained essentially constant. The system sits on the two-phase boiling curve throughout the cycles shown in Fig. 13, causing temperature and pressure to be extremely well correlated (Fig. 13a, b). Liquid flow is proportional to the pressure gradient and the vertical component of flow is mostly very well correlated with the fluid pressure (Fig. 13b). The
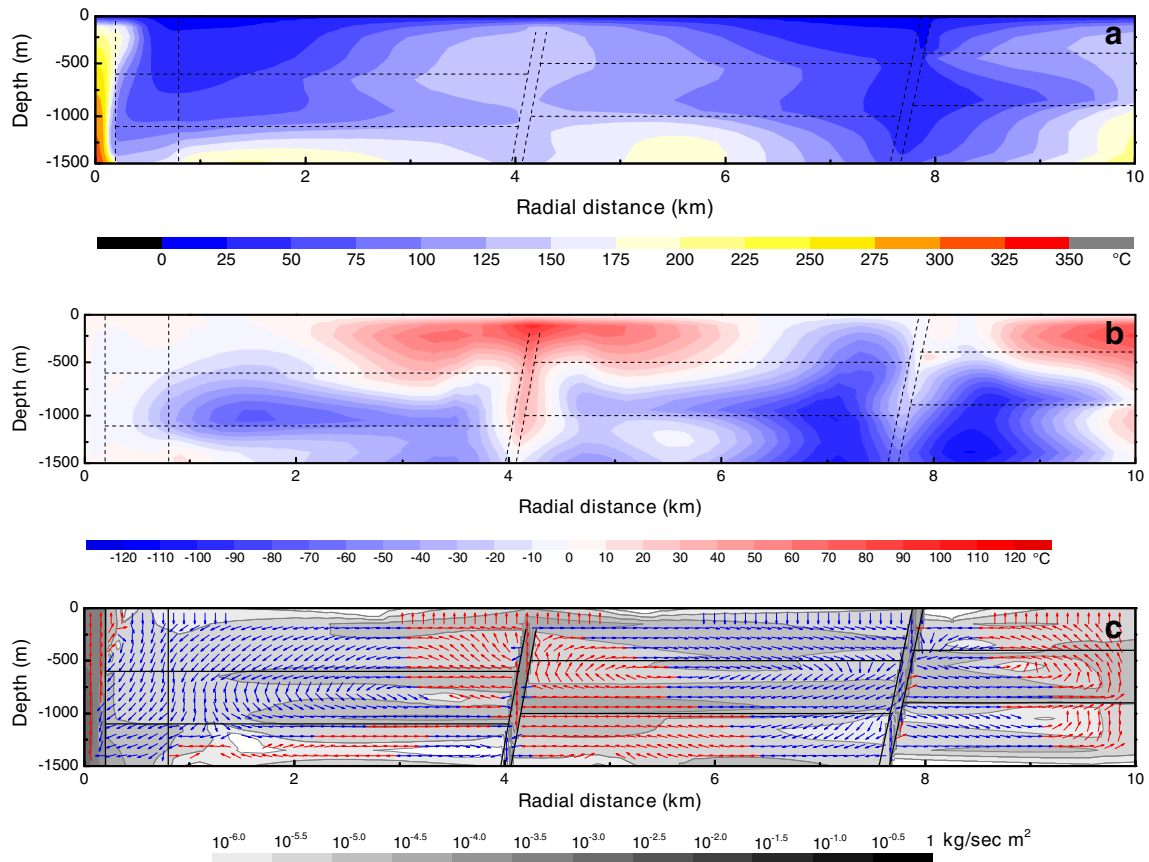
Fig. 9. Model 8 steady state results with two orders of magnitude increase in caldera-fill k_h: a) temperature distribution; b) temperature differences with respect to reference model with a wide warmer plume at depth < 500 m, whereas most of the domain is affected by cooling; c) flow field (see Fig. 3b for plotting details); increasing horizontal permeability by two orders of magnitude leads to pervasive advective flow.

upward flow of both gas and water (phase A) leads to a reduction of fluid pressure (Fig. 13b, c) and consequently temperature. Gas flux however is not well correlated with pressure (lag of ~5 years in first three cycles) indicating a complex coupling between pressure, water inflow and water phase transition (as reported by Woods, 1999).

The gas fraction within the gas-rich pockets fluctuates as a result of the constant basal heat flux and variable inflow of cooler water. The drop in fluid pressure at the monitoring point (P_1) (Fig. 12b$_3$) causes influx of cooler water from 110 years to 129 years (phase B). The drop in pressure and temperature reduces the amount of energy within the system inhibiting the production of gas (110 years). The balance between gas flux and gas production leads to a minimum of ~0.3 gas fraction at 129 years, when, concomitantly with the increase in pressure, discharge occurs (starting of cycle 2).

After 129 years the gas fraction never declines to reach the residual value (Fig. 13c); rather the inflow of water decreases in each cycle (Fig. 13b) depriving the system of the cooling effect due to the water influx (Fig. 13a). Vertical fluid flux dominates, although there is some recharge by lateral flow which in time becomes increasingly gas saturated because of the lateral extent of the basal gas generation zone (Fig. 13a$_4$–c$_4$). After 209 years, the pore space at P_1 is entirely gas and the temperature rises, reaching 400 °C by 275 years. Between 200 and 300 years there are three cycles in pressure and gas flux at P_1, which end the cyclic activity.

This simulation shows that increased heat flux along the base of the system causes the development of gas-rich pockets underneath a liquid-dominated hydrothermal system. An intrinsically unstable system develops, which, over time scale of c.100 years generates fluctuations in observable parameters that are related to the instability of the

water over gas distribution. However, as out of phase behaviour either side of fault B demonstrates, the timing of the instability cycles is controlled by both the permeability distribution in the caldera fill and boundary conditions.

5. Discussion

Campi Flegrei caldera has been recognised as one of the highest risk volcanic areas in the world and risk mitigation protocols are critical, but rely on understanding the physical processes during unrest. Despite significant research efforts it is unclear whether certain unrest signals (ground deformation, seismicity, degassing) are related to replenishment of the deep magmatic system or to magma cooling and fluid movement. Reducing the uncertainty related to the dynamics of the shallow hydrothermal system and the behaviour of rock under thermo-mechanical stress is as crucial as understanding the geometry and dynamics of the magma body.

By including faults in numerical simulations of hydrothermal systems we show that subsurface fluid flow can impact the temperature distribution within the caldera leading to sharp temperature gradients both vertically and horizontally. The recharge dynamics of the hydrothermal reservoir and the development of convective domains are also able to compartmentalize the effect of the input of magmatic fluids.

Two steep permeable faults at 4 and 7.5 km from the fumarole can provide routes for recharge of colder shallow groundwater. The flow direction within the faults is sensitive to fault zone permeability and the extent to which faults reach the surface (which promotes downward flow along the fault) or truncate in the subsurface, in which case their higher permeability may lead to upward flow. Different types of fault
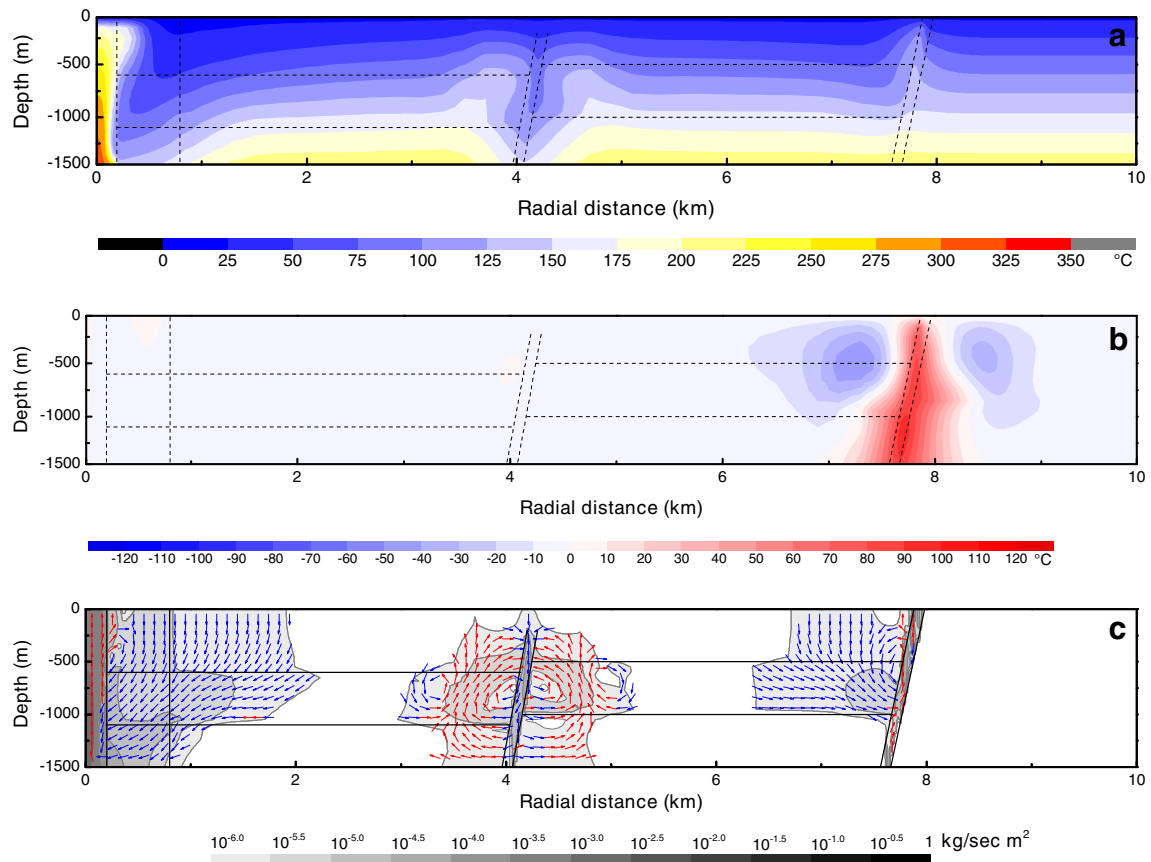
Fig. 10. Effect of caldera margin (model 9): a) temperature shows slight inversion of the isotherms along fault B; b) the combination of cooling along fault B in the reference model and upwelling of hot fluids in the current simulation produces a maximum temperature difference of 94 °C between this simulation and the reference model; c) fluid flow focuses on the hanging wall of fault B, whilst flow dynamics at <6 km radius are not affected by caldera margin.

are mapped in the field: deep regional structures, tensile fractures and caldera ring faults (Orsi et al., 1996; Acocella et al., 1999; Di Vito et al., 1999; Vitale and Isaia, 2014). Comparing these to the foci of degassing, ground deformation and volcano-tectonic events (e.g., Mofete and Solfatara areas, De Siena et al., 2010; Chiodini et al., 2010) indicates the primary role of non-ring faults and fractures in driving hot fluids towards the surface. Field data suggest that the caldera ring faults are relatively cold structures, inactive in terms of deformation and fluid discharge, in agreement with the preferential recharging role of fault B in our simulations.

However focussed discharge occurs along fault B in our model 9, where fault B represents the caldera margin bounded by low permeability rocks representing the root of the Apennine. There is no evidence in the field of preferential discharge along caldera ring faults, suggesting hydraulic connectivity between the caldera and the surrounding rock. Moreover the local hydraulic head follows a NE–SW alignment (Corrado et al., 1998) suggesting the presence of a lateral ground water recharge within the hydrothermal reservoir. Our 2D radial simulations are inadequate to capture the flow system far from the fumaroles, especially where intra-caldera faults isolate fumarole driven flow. A further complication is that to the south, groundwater and seawater mixing likely leads to significant changes in fluid density and favourable conditions for mineral precipitation which are not considered in our simulations. The results proposed in this paper are inevitably affected by the chosen geometry. Among other parameters, the depth and radius of the modelled domain and the aspect ratio of each rock layer might affect the results of the simulations altering the size and the shape of the convection cells. For instance, if the domain extended further, the fluid flow in the distal areas might split into more convective cells, altering the flow direction along fault B.

When faults act as focal points for fluid injection from deep reservoirs, buoyancy-driven discharge occurs on the hanging wall of faults. However whilst fault A in our simulations discharges fluids at the surface, fault B is a preferential route for influx of cool shallow groundwater. The different behaviour results from the combination of high permeability along faults and the infinite amount of cold water available at the top of the model. Fault B, which outcrops at the surface, enhances recharge, whereas 200 m of isotropic permeability overtops fault A, limiting recharge. Such an asymmetric plume, developed due to density-driven upwelling of fluids, has previously been described on the Pisciarelli fault by Chiodini et al. (2010). In the Solfatara area surficial fluid discharge occurs on the hanging wall. As suggested in Jung et al. (2014) for the CO_2 leakage on the Colorado Plateau (Utah), preferential discharge on the footwall is indicative of permeability barriers which divert flow from the hanging wall to the footwall. Detailed mapping of faults and fumarole distributions may constrain the relative permeabilities of foot wall and hanging wall at depth. With the exception Solfatara–Pisciarelli, there is a paucity of published data (Wohletz et al., 1999; Vaselli et al., 2011) on the distribution of fumaroles across the caldera. It appears that fumaroles focus around faults in the offshore portion of the caldera (Vaselli et al., 2011), and at the intersection between Apenninic and anti-Apenninic faults on land (Wohletz et al, 1999). Fluid emissions from offshore fumaroles and those onshore at Agnano, Mt. Nuovo and Serapeo are some 100 °C cooler than those at Solfatara–Pisciarelli (Vaselli et al., 2011), likely due to mixing with shallow waters. Advection might occur along the strike of the faults as rising magmatic fluids interact with cooler water inflow, however these 2D simulations are not able to capture the complexity of this process.

It is important to note that our definition of faults does not attempt to capture the complex geometries of fracture networks within the
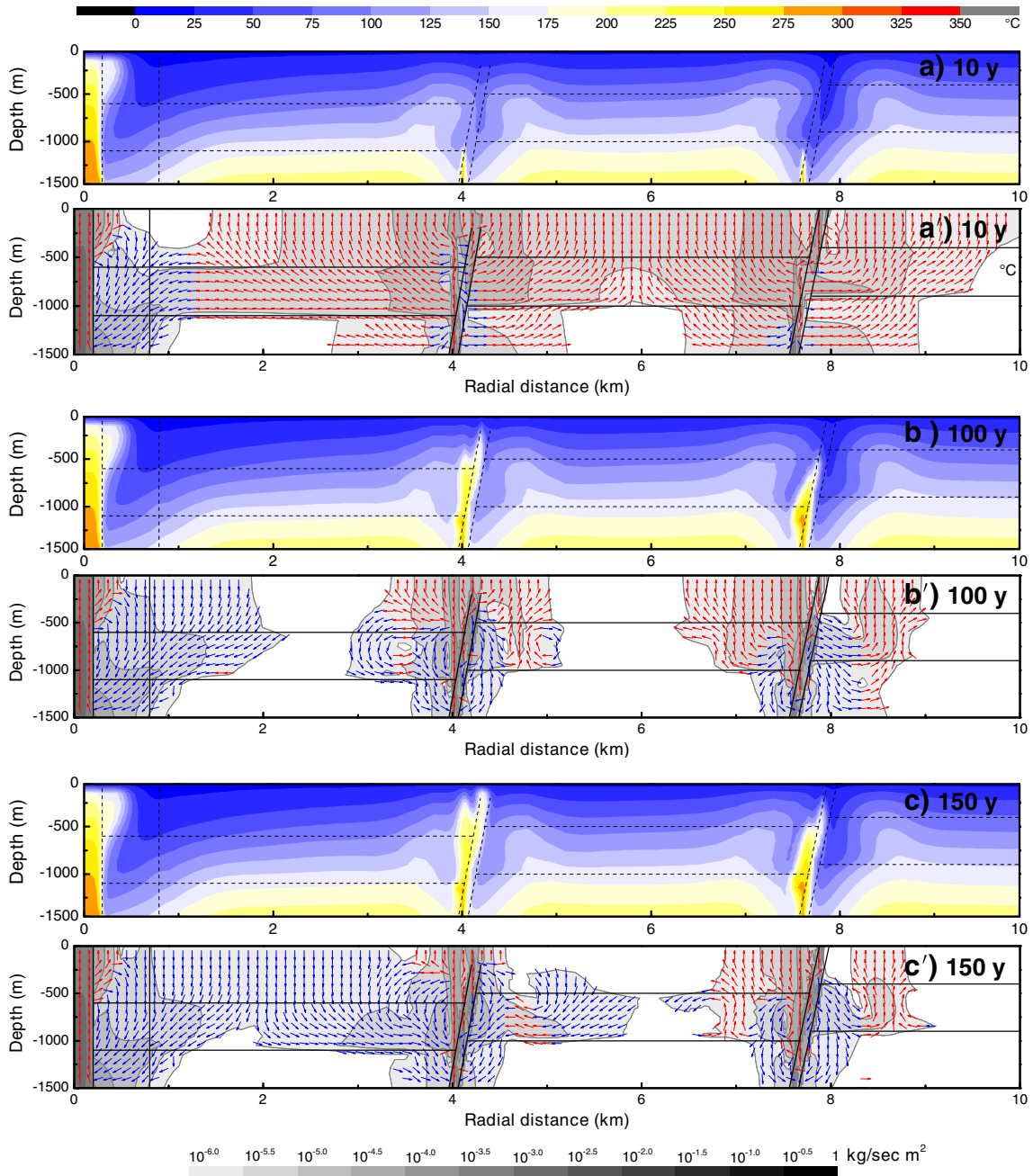
Fig. 11. Model 11, temporal evolution of temperature and flow within the caldera due to injection of fluids at faults and fumarole at crisis rate. (a) and (a′) show the discharge dominated scenario which lasts until the high temperature fluids reach the surface (b), (b′), (c) and (c′) show the later convective flow.

Campi Flegrei caldera but it captures the geometry of the main discontinuities of the system (caldera ring faults) and provides high permeability pathways to investigate the relationship between cool shallow groundwater and the hydrothermal reservoir. Furthermore, the porous media formulation of TOUGH2 is not appropriate for capturing the complexities of fluid flow within faults (Geiger and Matthäi, 2014). Faults also develop a complex 3D network that has not been captured in our 2D radial simulations. However the aim of our simulations is not to simulate a specific system but to evaluate the impact of faults.

We found that increasing horizontal permeability within the caldera fill leads to interaction between the previously separated flow cells and caused the horizontal component of flow to exceed the vertical one. Lateral flow within the hydrothermal reservoir may enhance mixing between superficial and deep waters leading to fluctuations in the fluid discharge temperature as well as the CO_2/H_2O ratio. Furthermore,

changes in fracture network and pore connectivity may enhance fluid flow, playing a key role in the release of pressure after inflation. For instance hydrofracturing due to the release of magmatic fluids can cause permeability "waves" that move through the system leading to a self-sustained pulsating behaviour (Weis, 2015). Our next step is coupling deformation and fluid flow to simulate whether ground deformation can be produced solely by changes of the flow pattern (Coco et al., submitted for publication).

We have demonstrated the sensitivity of hydrothermal systems to permeability structures, however there are many processes that can modify permeability in hydrologically open environments with high heat flux that we have not modelled. A potentially important one is water–rock interaction, which is a complex coupled process in which reactions are driven by flow across isotherms which are themselves a function of flow. Volcanoes in solfataric stage, including Campi Flegrei
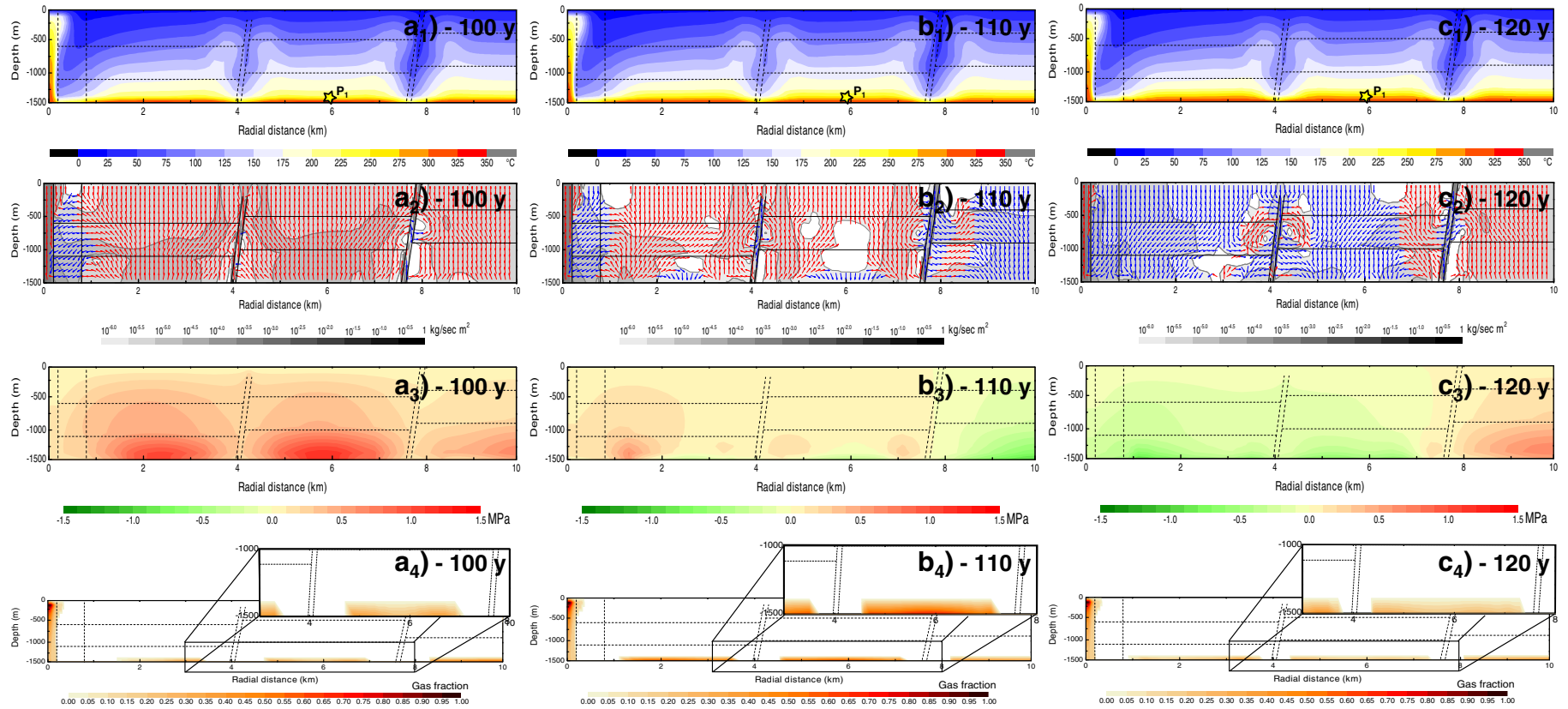
Fig. 12. Transient results from unrest model 12, with steady state model 2 conditions as initial conditions. Increasing the basal heat flux to 10 W/m² leads to heating along the base (a_1, b_1, c_1) and preferential discharge (a_2, b_2), but a switch in the flow dynamics is registered every 32 ± 5 years, as at 123 years (c_2). a_3, b_3 and c_3 show the increase in pore pressure (a_3) due to the generation of gas and drop due to gas flow (b_3) and cooling by water influx (c_3). a_4, b_4 and c_4 show the distribution of the gas phase. Point P_1 shows the location for which timeseries data are plotted in Fig. 13.
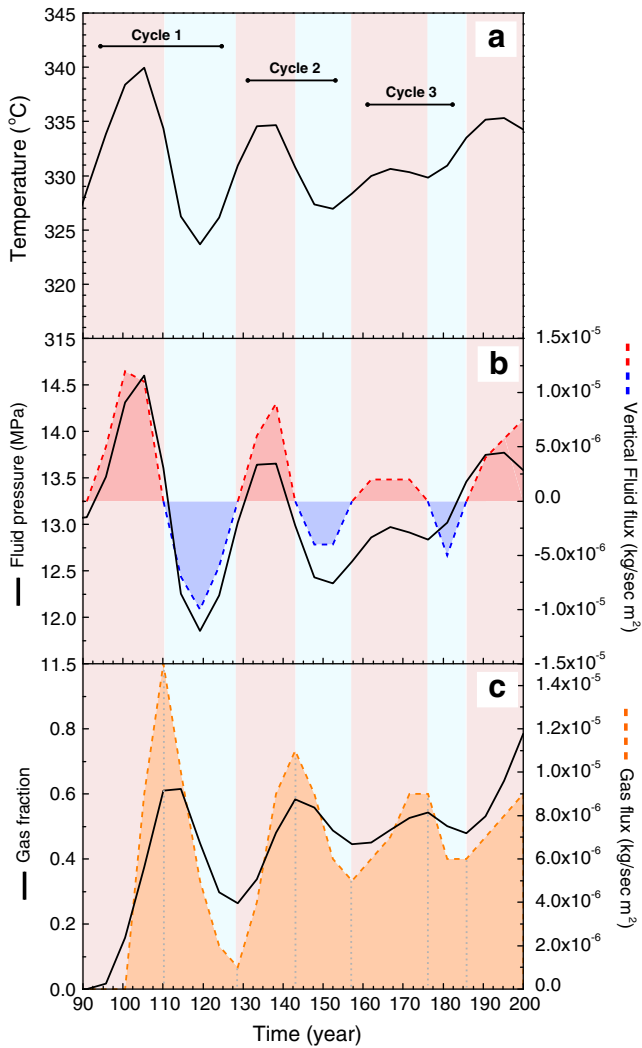
Fig. 13. Fluid characteristics as a function of time for model 12 at 1500 m depth and at a radial distance of 5900 m from fumarole (point P_1 in Fig. 12). Each cycle comprises upwards flow of both liquid and gas (phase A, light red background colour) and water inflow (phase B, light blue background colour). Temperature (a) and fluid pressure (b, black) are extremely well correlated because the water is boiling. Upwards (red) and downwards (blue) liquid flow are shown in "b"; negative fluid flux represents recharge. Maximum fluid pressure (black line) occurs before the peak in gas flux (c, orange) and gas fraction (c, black). (For interpretation of the references to colour in this figure legend, the reader is referred to the web version of this article.)

aquifer for which the dynamics, as well as interaction with the shallower system, are still unexplored.

In the quiet rate scenario (model 10), injected fluids reach the surface after 300 years. At the crisis rate (model 11), this time is reduced to less than 100 years (Fig. 15). High temperature fluid discharge occurs where faults breach the surface, whilst cooler groundwater circulates downward at each side of the faults to recharge the system. Field data suggest that magmatic fluids reach the surface in less than a year (Chiodini, 2009). However these measurements are at the fumaroles, which are relatively open conduits for flow. In contrast, our simulated faults are routes for cooler groundwater recharge (Fig. 4a). The upwelling of hot fluids is hence slowed by mixing with cooler superficial water. Furthermore vent opening may build high-transmissivity fractures which are not fully represented by our faults. Notwithstanding, changes in groundwater level and shallow groundwater temperature may forecast the location of new vents. For instance, a significant increase of pressure is registered near the surface after the beginning of the injection in model 11 (Fig. 15). After fluids reach the surface (100 years) a pressure drop is registered at 2 km and 6 km distance from the fumarole, which is between the fluid injection points. These pressure changes may lead to a recordable fluctuation of the water table or geodetic signal before the surficial hydrothermal manifestation. As suggested by the drop in fluid density recorded at the edge of the fumarole, the displacement of water by upwelling of gas leads to a drop in fluid density which can generate gravity signals.

The coupling of intense local heating, as in model 12 (high basal heat flux), and fluid flow develops a cyclicity (Fig. 13) comparable to the decennial cycles in ground deformation and seismicity at Campi Flegrei (Chiodini et al., 2010). The initial slow response of the system to perturbation is followed by a rapid discharge of fluids and the system develops a periodic behaviour (Fig. 13). Temperature increases until boiling occurs initiating the superficial discharge. This dissipates the overpressure allowing cooler groundwater recharge at depth. Cyclicity in ground deformation, seismicity and gas chemistry have previously been attributed to the periodic input of magmatic fluids, but our simulations offer another potential interpretation. However gas chemistry data (Chiodini et al., 2010) shows fluctuation within a 20 year period, which our simulation capture only partially (Fig. 14). If we consider the single-phase gas region at the fumarole as representative of the Solfatara discharge (Todesco et al., 2010) our simulation shows low impact on the CO_2/H_2O molar fraction. However at lower gas fraction (edge of the plume) any increase in steam is able to alter the composition of the gas phase leading to a drop in CO_2 up to 20% (e.g., 120 years) in agreement with the drop in CO_2 gas fraction during bradyseismic crises.

6. Conclusion

Numerical simulations of the Campi Flegrei hydrothermal system suggest that permeability architecture strongly impacts subsurface flow and temperature distributions. In particular, simulation results show that including geological complexity (i.e., faults and permeability anisotropy in the caldera fill), is necessary for the development of sharp horizontal temperature contrasts, which are observed in the field. Permeability contrasts between faults and caldera fill are also suggested to control the flow behaviour of faults which can either act as conduit for preferential discharge of high temperature fluids, or for influx of cool shallow groundwater. Understanding channelized flow will allow not only the development of more effective volcanic risk mitigation but also the identification of sites suitable for geothermal energy exploitation as recently on the Island of Montserrat (Poux and Brophy, 2012).

Simulations of magmatic unrest suggest that periodic geophysical and geochemical signals may result from stable boundary conditions due to the interaction between rising gas-rich pockets and descending recharge waters. Further simulations focused on constraining the main controlling parameters of the measured cyclicity of either ground
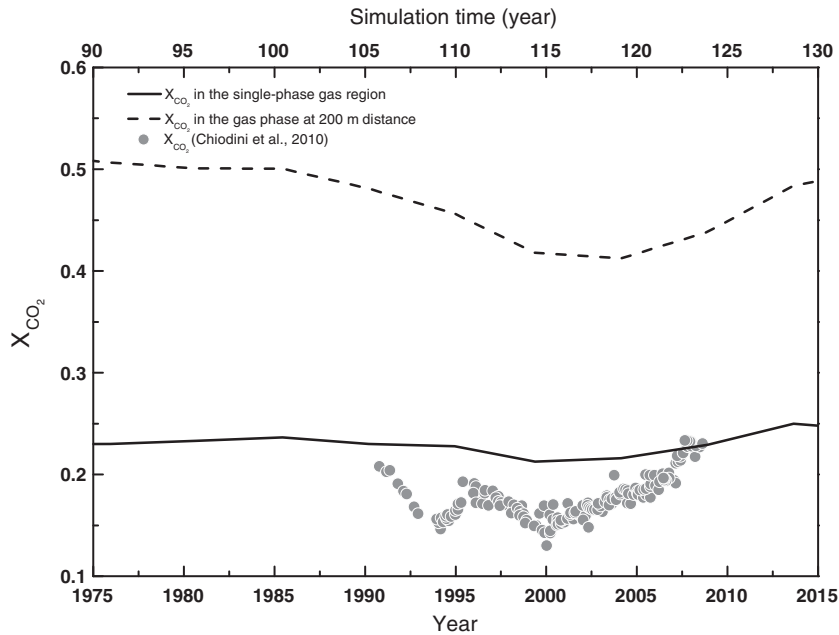
(Capaccioni and Mangani, 2001), often show extensive clay-rich deposits after acidic alteration of silicates, cross-cut by fine grained quartz deposits due to later precipitation of SiO_2 (Giggenbach, 1984, 1987; De Vivo et al., 1989; Henley and Berger, 2011). Hydrothermal alteration seems to preferentially reduce rock permeability (Tenthorey et al., 2003; Tenthorey and Fitz Gerald, 2006) potentially inhibiting degassing of the coupled magmatic–hydrothermal system as well as the extent of cool groundwater recharge. However, recent studies relating the temperatures and the permeabilities of the caldera fill deposits suggest that the Neapolitan Yellow Tuff becomes increasingly more permeable with increasing temperature as thermally unstable zeolites within the deposit become altered, whilst the Campanian Ignimbrite tuff, which underlies the modelled lithological sequence, remains unaffected due to the lack of those zeolite phases (Heap et al., 2014). The Campanian Ignimbrite tuff is one or two orders of magnitude more permeable than the Neapolitan Yellow Tuff (Heap et al., 2014) and is another

Fig. 14. Molar fraction of CO_2 (X_{CO_2}) in the single-phase gas region within the fumarolic plume at 150 m depth (solid line) and the X_{CO_2} in the gas phase at the edge of the plume (dashed line), where gas saturation never exceeds 0.5. We show 40 years of simulations (cycle 1). Circles are measured X_{CO_2} at Solfatara (Chiodini et al., 2010).

deformation, seismicity, gas emission might provide criteria to discriminate magmatic and hydrothermal unrest.

In model numbers 3, 10 and 11 hot plumes develop as a result of injection of fluids at the base of the faults. Although these plumes entrain groundwater as they rise, their radii do not exceed 2 km. Preferential discharge often occurs on the fault hanging wall in agreement with field evidence. However the lack of hydrothermal activity (fumaroles, hot springs) at the Campanian Ignimbrite caldera ring fault, compared
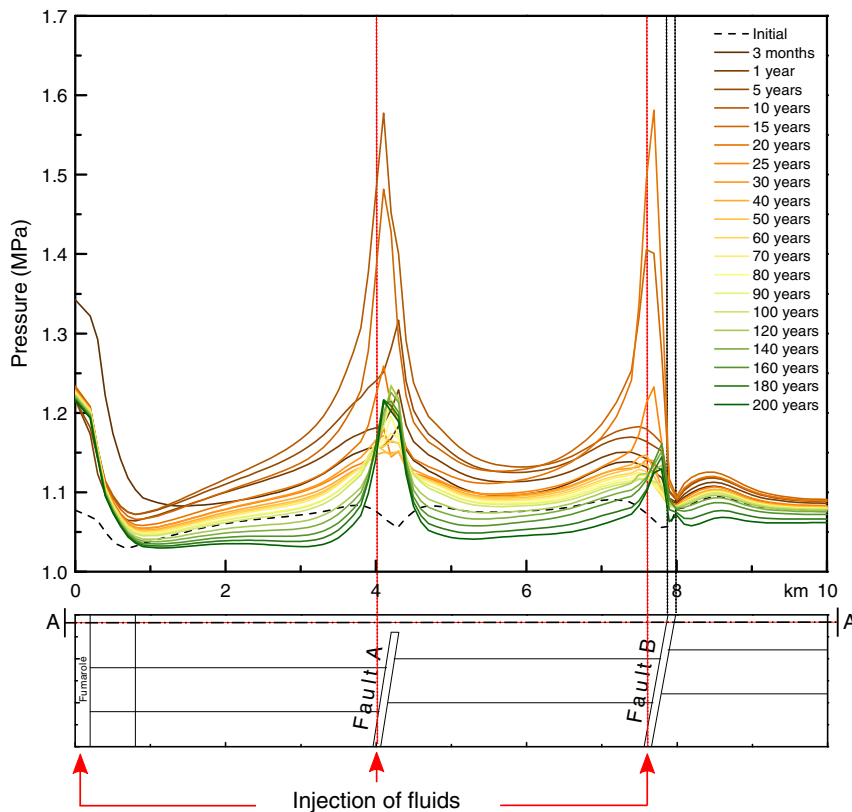

Fig. 15. Model 11: temporal evolution of pressure at 150 m depth (A–A′, profile near the surface) during the first 200 years. Injection points are highlighted by red arrows. (For interpretation of the references to colour in this figure legend, the reader is referred to the web version of this article.)

with the simulation number 9 results, suggests hydraulic continuity between the caldera fill and the outer domain.

Acknowledgement

References

Acocella, V., Salvini, F., Funiciello, R., Faccenna, C., 1999. The role of transfer structures on volcanic activity at Campi Flegrei (Southern Italy). J. Volcanol. Geotherm. Res. 91, 123–139. http://dx.doi.org/10.1016/S0377-0273(99)00032-3.

Acocella, V., Gudmundsson, A., Funiciello, R., 2000. Interaction and linkage of extension fractures and normal faults: examples from the rift zone of Iceland. J. Struct. Geol. 22, 1233–1246. http://dx.doi.org/10.1016/S0191-8141(00)00031-6.

Amoruso, A., Crescentini, L., Berrino, G., 2008. Simultaneous inversion of deformation and gravity changes in a horizontally layered half-space: evidences for magma intrusion during the 1982–1984 unrest at Campi Flegrei caldera (Italy). Earth Planet. Sci. Lett. 272, 181–188. http://dx.doi.org/10.1016/j.epsl.2008.04.040.

Arienzo, I., Moretti, R., Civetta, L., Orsi, G., Papale, P., 2010. The feeding system of Agnano–Monte Spina eruption (Campi Flegrei, Italy): dragging the past into present activity and future scenarios. Chem. Geol. 270, 135–147. http://dx.doi.org/10.1016/j.chemgeo.2009.11.012.

Barberi, F., Innocenti, F., Lirer, L., Munno, R., Pescatore, T., Santacroce, R., 1978. The Campanian Ignimbrite: a major prehistoric eruption in the Neapolitan area (Italy). Bull. Volcanol. 41, 1–22.

Battaglia, M., Troise, C., Obrizzo, F., Pingue, F., De Natale, G., 2006. Evidence for fluid migration as the source of deformation at Campi Flegrei caldera (Italy). Geophys. Res. Lett. 33, L01307. http://dx.doi.org/10.1029/2005GL024904.

Berrino, G., 1994. Gravity changes induced by height mass variations at the Campi-Flegrei caldera. J. Volcanol. Geotherm. Res. 61, 293–309. http://dx.doi.org/10.1016/0377-0273(94)90010-8.

Bodnar, R.J., Cannatelli, C., De Vivo, B., Lima, A., Belkin, H.E., Milia, A., 2007. Quantitative model for magma degassing and ground deformation (bradyseism) at Campi Flegrei, Italy: implications for future eruptions. Geology 35, 791–794. http://dx.doi.org/10.1130/G23653A.1.

Bodvarsson, G.S., Benson, S.M., Witherspoon, P.A., 1982. Theory of the development of geothermal systems charged by vertical faults. J. Geophys. Res. 87, 9317–9328. http://dx.doi.org/10.1029/jb087ib11p09317.

Bonafede, M., 1991. Hot fluid migration — an efficient source of ground deformation — application to the 1982–1985 crisis at Campi Flegrei—Italy. J. Volcanol. Geotherm. Res. 48, 187–198. http://dx.doi.org/10.1016/0377-0273(91)90042-X.

Bonafede, M., Dragoni, M., Quareni, F., 1986. Displacement and stress-fields produced by a center of dilation and by a pressure source in a viscoelastic half-space — application to the study of ground deformation and seismic activity at Campi-Flegrei, Italy. Geophys. J. Int. 87, 455–485. http://dx.doi.org/10.1111/j.1365-246X.1986.tb06632.x.

Bruno, P.P.G., Ricciardi, G.P., Petrillo, Z., Di Fiore, V., Troiano, A., Chiodini, G., 2007. Geophysical and hydrogeological experiments from a shallow hydrothermal system at Solfatara Volcano, Campi Flegrei, Italy: response to caldera unrest. J. Geophys. Res. Solid Earth 112, B06201. http://dx.doi.org/10.1029/2006jb004383.

Caliro, S., Chiodini, G., Moretti, R., Avino, R., Granieri, D., Russo, M., Fiebig, J., 2007. The origin of the fumaroles of La Solfatara (Campi Flegrei, South Italy). Geochim. Cosmochim. Acta 71, 3040–3055. http://dx.doi.org/10.1016/j.gca.2007.04.007.

Capaccioni, B., Mangani, F., 2001. Monitoring of active but quiescent volcanoes using light hydrocarbon distribution in volcanic gases: the results of 4 years of discontinuous monitoring in the Campi Flegrei (Italy). Earth Planet. Sci. Lett. 188, 543–555. http://dx.doi.org/10.1016/S0012-821X(01)00338-7.

Capuano, P., Russo, G., Civetta, L., Orsi, G., D'Antonio, M., Moretti, R., 2013. The active portion of the Campi Flegrei caldera structure imaged by 3-D inversion of gravity data. Geochem. Geophys. Geosyst. 14, 4681–4697. http://dx.doi.org/10.1002/ggge.20276.

Carella, R., Guglielminetti, M., 1983. Multiple reservoirs in the Mofete fields, Naples, Italy. Workshop on Geothermal Reservoir Engineering. Stanford (12 pp.).

Carlino, S., Somma, R., Troise, C., De Natale, G., 2012. The geothermal exploration of Campanian volcanoes: historical review and future development. Renew. Sustain. Energy Rev. 16, 1004–1030. http://dx.doi.org/10.1016/j.rser.2011.09.023.

Chelini, W., Sbrana, A., 1987. Subsurface geology. In: Rosi, M., Sbrana, A. (Eds.), Phlegrean Fields. Quaderni della Ricerca Scientifica, pp. 94–102.

Chiodini, G., 2009. CO_2/CH_4 ratio in fumaroles a powerful tool to detect magma degassing episodes at quiescent volcanoes. Geophys. Res. Lett. 36, L02302. http://dx.doi.org/10.1029/2008GL036347.

Chiodini, G., Marini, L., 1998. Hydrothermal gas equilibria: the $H_2O–H_2–CO_2–CO–CH_4$ system. Geochim. Cosmochim. Acta 62, 2673–2687. http://dx.doi.org/10.1016/S0016-7037(98)00181-1.

Chiodini, G., Frondini, F., Cardellini, C., Granieri, D., Marini, L., Ventura, G., 2001. CO_2 degassing and energy release at Solfatara volcano, Campi Flegrei, Italy. J. Geophys. Res. Solid Earth 106, 16213–16221. http://dx.doi.org/10.1029/2001JB000246.

Chiodini, G., Todesco, M., Caliro, S., Del Gaudio, C., Macedonio, G., Russo, M., 2003. Magma degassing as a trigger of bradyseismic events: the case of Phlegrean Fields (Italy). Geophys. Res. Lett. 30, 171–174. http://dx.doi.org/10.1029/2002GL016790.

Chiodini, G., Caliro, S., Cardellini, C., Granieri, D., Avino, R., Baldini, A., Donnini, M., Minopoli, C., 2010. Long-term variations of the Campi Flegrei, Italy, volcanic system as revealed by the monitoring of hydrothermal activity. J. Geophys. Res. Solid Earth 115, B03205. http://dx.doi.org/10.1029/2008jb006258.

Chiodini, G., Caliro, S., De Martino, P., Avino, R., Gherardi, F., 2012. Early signals of new volcanic unrest at Campi Flegrei caldera? Insights from geochemical data and physical simulations. Geology 40, 943–946. http://dx.doi.org/10.1130/G33251.1.

Civetta, L., Orsi, G., Pappalardo, L., Fisher, R.V., Heiken, G., Ort, M., 1997. Geochemical zoning, mingling, eruptive dynamics and depositional processes — the Campanian Ignimbrite, Campi Flegrei caldera, Italy. J. Volcanol. Geotherm. Res. 75, 183–219. http://dx.doi.org/10.1016/S0377-0273(96)00027-3.

Coco, A., Gottsmann, J., Whitaker, F., Rust, A., Currenti, G., Jasim, A., Bunney, S., 2015. Numerical models for ground deformation and gravity changes during volcanic unrest: simulating the hydrothermal system dynamics of an active caldera. J. Geophys. Res. Solid Earth (submitted for publication June).

Corrado, G., Lorenzo, S.D., Mongelli, F., Tramacere, A., Zito, G., 1998. Surface heat flow density at the phlegrean fields caldera (Southern Italy). Geothermics 27, 469–484. http://dx.doi.org/10.1016/S0375-6505(98)00023-6.

De Martino, P., Tammaro, U., Obrizzo, F., 2014. Gps time series at Campi Flegrei caldera (2000–2013). Ann. Geophys. 57. http://dx.doi.org/10.4401/ag-6431.

De Natale, G., Pingue, F., 1993. Ground deformations in collapsed caldera structures. J. Volcanol. Geotherm. Res. 57, 19–38. http://dx.doi.org/10.1016/0377-0273(93)90029-Q.

De Natale, G., Petrazzuoli, S.M., Pingue, F., 1997. The effect of collapse structures on ground deformations in calderas. Geophys. Res. Lett. 24, 1555–1558. http://dx.doi.org/10.1029/97GL01600.

De Natale, G., Troise, C., Pingue, F., 2001. A mechanical fluid-dynamical model for ground movements at Campi Flegrei caldera. J. Geodyn. 32, 487–517. http://dx.doi.org/10.1016/S0264-3707(01)00045-X.

De Siena, L., Del Pezzo, E., Bianco, F., 2010. Seismic attenuation imaging of Campi Flegrei: evidence of gas reservoirs, hydrothermal basins, and feeding systems. J. Geophys. Res. Solid Earth 115, B09312. http://dx.doi.org/10.1029/2009jb006938.

De Vivo, B., Belkin, H.E., Barbieri, M., Chelini, W., Lattanzi, P., Lima, A., Tolomeo, L., 1989. The Campi Flegrei (Italy) geothermal system: a fluid inclusion study of the Mofete and San Vito fields. J. Volcanol. Geotherm. Res. 36, 303–326. http://dx.doi.org/10.1016/0377-0273(89)90076-0.

De Vivo, B., Rolandi, G., Gans, P.B., Calvert, A., Bohrson, W.A., Spera, F.J., Belkin, H.E., 2001. New constraints on the pyroclastic eruptive history of the Campanian volcanic Plain (Italy). Mineral. Petrol. 73, 47–65. http://dx.doi.org/10.1007/s007100170010.

Deino, A.L., Orsi, G., de Vita, S., Piochi, M., 2004. The age of the Neapolitan Yellow Tuff caldera-forming eruption (Campi Flegrei caldera Italy) assessed by Ar^{40}/Ar^{39} dating method. J. Volcanol. Geotherm. Res. 133, 157–170. http://dx.doi.org/10.1016/S0377-0273(03)00396-2.

Di Vito, M., Lirer, L., Mastrolorenzo, G., Rolandi, G., 1987. The 1538 Monte Nuovo eruption (Campi Flegrei, Italy). Bull. Volcanol. 49, 608–615. http://dx.doi.org/10.1007/BF01079966.

Di Vito, M.A., Isaia, R., Orsi, G., Southon, J., de Vita, S., D'Antonio, M., Pappalardo, L., Piochi, M., 1999. Volcanism and deformation since 12,000 years at the Campi Flegrei caldera (Italy). J. Volcanol. Geotherm. Res. 91, 221–246. http://dx.doi.org/10.1016/S0377-0273(99)00037-2.

Dvorak, J.J., Mastrolorenzo, G., 1991. The mechanisms of recent vertical crustal movements in Campi Flegrei caldera, southern Italy. Am. Spec. Pap. 263, 1–47.

Dzurisin, D., Newhall, C.G., 1984. Recent seismicity and ground deformation at Long Valley (California), Yellowstone (Wyoming), the Phlegraean Fields (Italy), and Rabaul (Papua New Guinea). In: Hill, D.P., Bailey, R.A., Ryall, A.S. (Eds.), Active Tectonic and Magmatic Processes Beneath Long Valley Caldera, Eastern California, U.S. Geological Survey Open-File Report. 84-939, pp. 784–829.

Fisher, R.V., Orsi, G., Ort, M., Heiken, G., 1993. Mobility of large-volume pyroclastic flow — emplacement of the Campanian Ignimbrite, Italy. J. Volcanol. Geotherm. Res. 56, 205–220. http://dx.doi.org/10.1016/0377-0273(93)90017-L.

Folch, A., Gottsmann, J., 2006. Volcanic unrest: faults and ground uplift at active calderas. In: Troise, C., Natale, G.D., Kilburn, C.R.J. (Eds.), Mechanisms of Activity and Unrest at Large Calderas. Geological Society of London.

Fournier, R.O., 1999. Hydrothermal processes related to movement of fluid from plastic into brittle rock in the magmatic-epithermal environment. Econ. Geol.Bull.Econ. Geol. 94, 1193–1211. http://dx.doi.org/10.2113/gsecongeo.94.8.1193.

Gaeta, F.S., De Natale, G., Peluso, F., Mastrolorenzo, G., Castagnolo, D., Troise, C., Pingue, F., Mita, D.G., Rossano, S., 1998. Genesis and evolution of unrest episodes at Campi Flegrei caldera: the role of thermal fluid-dynamical processes in the geothermal system. J. Geophys. Res. Solid Earth 103, 20921–20933. http://dx.doi.org/10.1029/97JB03294.

Geiger, S., Matthäi, S., 2014. What can we learn from high-resolution numerical simulations of single- and multi-phase fluid flow in fractured outcrop analogues? Geol. Soc. Lond., Spec. Publ. 374, 125–144. http://dx.doi.org/10.1144/SP374.8.

Giggenbach, W.F., 1984. Mass-transfer in hydrothermal alteration systems — a conceptual-approach. Geochim. Cosmochim. Acta 48, 2693–2711. http://dx.doi.org/10.1016/0016-7037(84)90317-X.

Giggenbach, W.F., 1987. Redox processes governing the chemistry of fumarolic gas discharges from White Island, New Zealand. Appl. Geochem. 2, 143–161. http://dx.doi.org/10.1016/0883-2927(87)90030-8.

Gottsmann, J., Martí, J., 2008. Caldera volcanism: analysis, modelling and response. Developments in Volcanology 10. Elsevier (ISBN 978-0-444-53165-0).

Gottsmann, J., Rymer, H., Berrino, G., 2006. Unrest at the Campi Flegrei caldera (Italy): a critical evaluation of source parameters from geodetic data inversion. J. Volcanol. Geotherm. Res. 150, 132–145. http://dx.doi.org/10.1016/j.jvolgeores.2005.07.002.

Goyal, K.P., Narasimhan, T.N., 1982. Heat and mass-transfer in a fault-controlled geothermal reservoir charged at constant pressure. J. Geophys. Res. 87, 8581–8590. http://dx.doi.org/10.1029/JB087iB10p08581.

Guidoboni, E., Ciuccarelli, C., 2011. The Campi Flegrei caldera: historical revision and new data on seismic crises, bradyseisms, the Monte Nuovo eruption and ensuing earthquakes (twelfth century 1582 AD). Bull. Volcanol. 73, 655–677. http://dx.doi.org/10.1007/s00445-010-0430-3.

Heap, M.J., Baud, P., Meredith, P.G., Vinciguerra, S., Reuschle, T., 2014. The permeability and elastic moduli of tuff from Campi Flegrei, Italy: implications for ground deformation modelling. Solid Earth 5, 25–44. http://dx.doi.org/10.5194/se-5-25-2014.

Henley, R.W., Berger, B.R., 2011. Magmatic-vapor expansion and the formation of high-sulfidation gold deposits: chemical controls on alteration and mineralization. Ore Geol. Rev. 39, 63–74. http://dx.doi.org/10.1016/j.oregeorev.2010.11.003.

Isaia, R., Marianelli, P., Sbrana, A., 2009. Caldera unrest prior to intense volcanism in Campi Flegrei (Italy) at 4.0 ka BP: implications for caldera dynamics and future eruptive scenarios. Geophys. Res. Lett. 36, L21303. http://dx.doi.org/10.1029/2009GL040513.

Jung, N.H., Han, W.S., Watson, Z.T., Graham, J.P., Kim, K.Y., 2014. Fault-controlled CO_2 leakage from natural reservoirs in the Colorado Plateau, East-Central Utah. Earth Planet. Sci. Lett. 403, 358–367. http://dx.doi.org/10.1016/j.epsl.2014.07.012.

Kilty, K., Chapman, D.S., Mase, C.W., 1979. Forced convective heat-transfer in the Monroe hot springs geothermal system. J. Volcanol. Geotherm. Res. 6, 257–277. http://dx.doi.org/10.1016/0377-0273(79)90005-2.

Lipman, P.W., 2007. Incremental assembly and prolonged consolidation of Cordilleran magma chambers: evidence from the Southern Rocky Mountain volcanic field. Geosphere 3, 42–70. http://dx.doi.org/10.1130/GES00061.1.

Murphy, H.D., 1979. Convective instabilities in vertical fractures and faults. J. Geophys. Res. 84, 6121–6130. http://dx.doi.org/10.1029/jb084ib11p06121.

Newhall, C.G., Dzurisin, D., 1988. Historical unrest at large calderas of the world. Bulletin 1855. U. S. Geol. Surv. 2 (1108 pp.).

Orsi, G., D'Antonio, M., de Vita, S., Gallo, G., 1992. The Neapolitan Yellow Tuff, a large-magnitude trachytic phreatoplinian eruption: eruptive dynamics, magma withdrawal and caldera collapse. J. Volcanol. Geotherm. Res. 53, 275–287. http://dx.doi.org/10.1016/0377-0273(92)90086-S.

Orsi, G., de Vita, S., Di Vito, M., 1996. The restless, resurgent Campi Flegrei nested caldera (Italy): constraints on its evolution and configuration. J. Volcanol. Geotherm. Res. 74, 179–214. http://dx.doi.org/10.1016/S0377-0273(96)00063-7.

Orsi, G., Civetta, L., Del Gaudio, C., de Vita, S., Di Vito, R.A., Isaia, R., Petrazzuoli, S.M., Ricciardi, G.P., Ricco, C., 1999. Short-term ground deformations and seismicity in the resurgent Campi Flegrei caldera (Italy): an example of active block-resurgence in a densely populated area. J. Volcanol. Geotherm. Res. 91, 415–451. http://dx.doi.org/10.1016/S0377-0273(99)00050-5.

Orsi, G., Di Vito, M., Isaia, R., 2004. Volcanic hazard assessment at the restless Campi Flegrei caldera. Bull. Volcanol. 66, 514–530. http://dx.doi.org/10.1007/s00445-003-0336-4.

Peluso, F., Arienzo, I., 2007. Experimental determination of permeability of Neapolitan yellow tuff. J. Volcanol. Geotherm. Res. 160, 125–136. http://dx.doi.org/10.1016/j.jvolgeores.2006.09.004.

Petrillo, Z., Chiodini, G., Mangiacapra, A., Caliro, S., Capuano, P., Russo, G., Cardellini, C., Avino, R., 2013. Defining a 3D physical model for the hydrothermal circulation at Campi Flegrei caldera (Italy). J. Volcanol. Geotherm. Res. 264, 172–182. http://dx.doi.org/10.1016/j.jvolgeores.2013.08.008.

Piochi, M., Kilburn, C.R.J., Vito, M.A., Mormone, A., Tramelli, A., Troise, C., Natale, G., 2014. The volcanic and geothermally active Campi Flegrei caldera: an integrated multidisciplinary image of its buried structure. Int. J. Earth Sci. 103, 401–421. http://dx.doi.org/10.1007/s00531-013-0972-7.

Poux, B., Brophy, P., 2012. Geothermal Exploration on the Island of Montserrat. 36. GRC Transactions, Caribbean, pp. 737–744.

Pruess, K., Oldenburg, C., Moridis, G., 1999. TOUGH2 User's Guide, Version 2.0, Lawrence Berkeley National Laboratory Report LBNL-43134. Berkeley, CA (208 pp.).

Rinaldi, A.P., Todesco, M., Bonafede, M., 2010. Hydrothermal instability and ground displacement at the Campi Flegrei caldera. Phys. Earth Planet. Inter. 178, 155–161. http://dx.doi.org/10.1016/j.pepi.2009.09.005.

Rinaldi, A.P., Todesco, M., Vandemeulebrouck, J., Revil, A., Bonafede, M., 2011. Electrical conductivity, ground displacement, gravity changes, and gas flow at Solfatara crater (Campi Flegrei caldera, Italy): results from numerical modeling. J. Volcanol. Geotherm. Res. 207, 93–105. http://dx.doi.org/10.1016/j.jvolgeores.2011.07.008.

Rosi, M., Sbrana, A., 1987. Phlegrean Fields CNR, Quaderni della Ricerca Scientifica. 114 (175 pp.).

Rosi, M., Vezzoli, L., Aleotti, P., De Cenzi, M., 1996. Interaction between caldera collapse and eruptive dynamics during the Campanian Ignimbrite eruption, Phlegraean Fields, Italy. Bull. Volcanol. 57, 541–554. http://dx.doi.org/10.1007/BF00304438.

Rosi, M., Vezzoli, L., Castelmenzano, A., Grieco, G., 1999. Plinian pumice fall deposit of the Campanian Ignimbrite eruption (Phlegraean Fields, Italy). J. Volcanol. Geotherm. Res. 91, 179–198. http://dx.doi.org/10.1016/S0377-0273(99)00035-9.

Rubin, A.M., 1995. Getting granite dikes out of the source region. J. Geophys. Res. Solid Earth 100, 5911–5929. http://dx.doi.org/10.1029/94JB02942.

Saunders, S.J., 2004. The possible contribution of circumferential fault intrusion to caldera resurgence. Bull. Volcanol. 67, 57–71. http://dx.doi.org/10.1007/s00445-004-0360-z.

Tenthorey, E., Fitz Gerald, J.D., 2006. Feedbacks between deformation, hydrothermal reaction and permeability evolution in the crust: experimental insights. Earth Planet. Sci. Lett. 247, 117–129. http://dx.doi.org/10.1016/j.epsl.2006.05.005.

Tenthorey, E., Cox, S.F., Todd, H.F., 2003. Evolution of strength recovery and permeability during fluid–rock reaction in experimental fault zones. Earth Planet. Sci. Lett. 206, 161–172. http://dx.doi.org/10.1016/S0012-821X(02)01082-8.

Todesco, M., Berrino, G., 2005. Modeling hydrothermal fluid circulation and gravity signals at the Phlegraean Fields caldera. Earth Planet. Sci. Lett. 240, 328–338. http://dx.doi.org/10.1016/j.epsl.2005.09.016.

Todesco, M., Chiodini, G., Macedonio, G., 2003. Monitoring and modelling hydrothermal fluid emission at La Solfatara (Phlegrean Fields, Italy). An interdisciplinary approach to the study of diffuse degassing. J. Volcanol. Geotherm. Res. 125, 57–79. http://dx.doi.org/10.1016/S0377-0273(03)00089-1.

Todesco, M., Rutqvist, J., Chiodini, G., Pruess, K., Oldenburg, C.I.M., 2004. Modeling of recent volcanic episodes at Phlegrean Fields (Italy): geochemical variations and ground deformation. Geothermics 33, 531–547. http://dx.doi.org/10.1016/j.geothermics.2003.08.014.

Todesco, M., Rinaldi, A.P., Bonafede, M., 2010. Modeling of unrest signals in heterogeneous hydrothermal systems. J. Geophys. Res. Solid Earth 115. http://dx.doi.org/10.1029/2010jb007474 B09213.

Townend, J., Zoback, M.D., 2000. How faulting keeps the crust strong. Geology 28, 399–402. http://dx.doi.org/10.1130/0091-7613(2000)28<399:Hfktcs>2.0.Co;2.

Troise, C., DeNatale, G., Pingue, F., Zollo, A., 1997. A model for earthquake generation during unrest episodes at Campi Flegrei and Rabaul calderas. Geophys. Res. Lett. 24, 1575–1578. http://dx.doi.org/10.1029/97GL01477.

Troise, C., De Natale, G., Pingue, F., Tammaro, U., DeMartino, P., Obrizzo, F., Boschi, E., 2008. A new uplift episode at Campi Flegrei Caldera (Southern Italy): implications for unrest interpretation and eruption hazard evaluation. In Caldera Volcanism: Analysis, Modelling and Response. Dev. Volcanol. 10, 375–392.

Vanorio, T., Virieux, J., Capuano, P., Russo, G., 2005. Three-dimensional seismic tomography from P wave and S wave microearthquake travel times and rock physics characterization of the Campi Flegrei Caldera. J. Geophys. Res. Solid Earth 110, B03201. http://dx.doi.org/10.1029/2004jb003102.

Vaselli, O., Tassi, F., Tedesco, D., Poreda, R.J., Caprai, A., 2011. Submarine and inland gas discharges from the Campi Flegrei (Southern Italy) and the Pozzuoli Bay: geochemical clues for a common hydrothermal–magmatic source. Procedia Earth Planet. Sci. 4, 57–73. http://dx.doi.org/10.1016/j.proeps.2011.11.007.

Vitale, S., Isaia, R., 2014. Fractures and faults in volcanic rocks (Campi Flegrei, southern Italy): insight into volcano-tectonic processes. Int. J. Earth Sci. 103, 801–819. http://dx.doi.org/10.1007/s00531-013-0979-0.

Weis, P., 2015. The dynamic interplay between saline fluid flow and rock permeability in magmatic-hydrothermal systems. Geofluids 15, 350–371. http://dx.doi.org/10.1111/gfl.12100.

Wohletz, K., Orsi, G., de Vita, S., 1995. Eruptive mechanisms of the Neapolitan Yellow Tuff interpreted from stratigraphic, chemical and granulometric data. J. Volcanol. Geotherm. Res. 67, 263–290. http://dx.doi.org/10.1016/0377-0273(95)00002-C.

Wohletz, K., Civetta, L., Orsi, G., 1999. Thermal evolution of the Phlegraean magmatic system. J. Volcanol. Geotherm. Res. 91, 381–414. http://dx.doi.org/10.1016/S0377-0273(99)00048-7.

Woods, A.W., 1999. Liquid and vapor flow in superheated rock. Annu. Rev. Fluid Mech. 31, 171–199. http://dx.doi.org/10.1146/annurev.fluid.31.1.171.

Wright, H.M., Cashman, K.V., 2014. Compaction and gas loss in welded pyroclastic deposits as revealed by porosity, permeability, and electrical conductivity measurements of the Shevlin Park Tuff. Geol. Soc. Am. Bull. 126, 234–247. http://dx.doi.org/10.1016/0377-0273(95)00002-C.

Zollo, A., Maercklin, N., Vassallo, M., Dello Iacono, D., Virieux, J., Gasparini, P., 2008. Seismic reflections reveal a massive melt layer feeding Campi Flegrei caldera. Geophys. Res. Lett. 35, L12306. http://dx.doi.org/10.1029/2008GL034242.